Article

Cell Stem Cell

Human iPSC Glial Mouse Chimeras Reveal Glial Contributions to Schizophrenia

Graphical Abstract

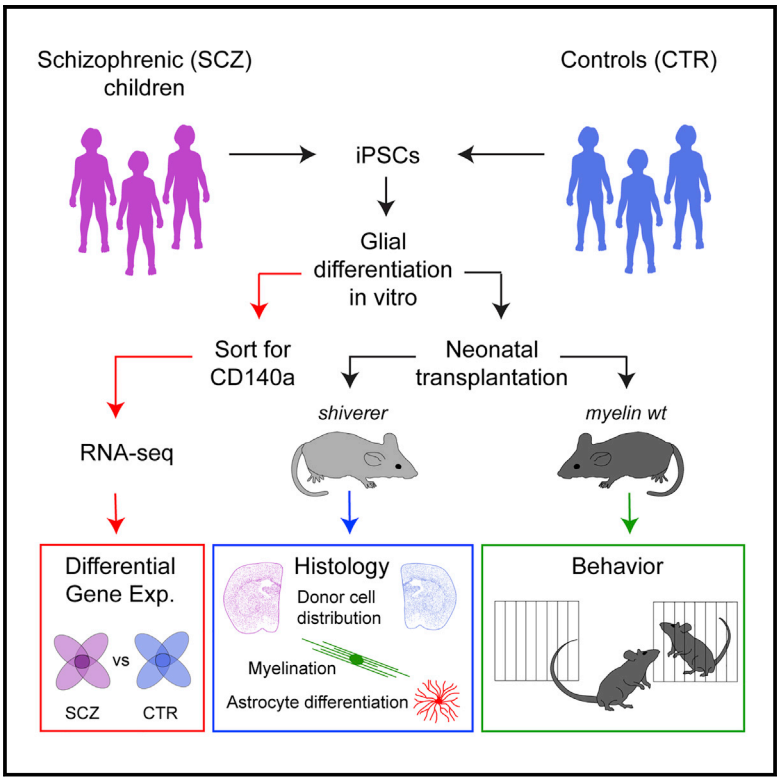

Authors

Martha S. Windrem, Mikhail Osipovitch, Zhengshan Liu, ..., Robert L. Findling, Paul J. Tesar, Steven A. Goldman

Correspondence

steven_goldman@urmc.rochester.edu or goldman@sund.ku.dk

In Brief

Goldman and colleagues use mice chimerized with human patient-derived glial progenitor cells to find out whether glia contribute to childhood-onset schizophrenia. The defects in cell differentiation, myelination, and behavior they see strongly suggest that glial cells do, in fact, have a previously unappreciated role in the pathogenesis of this disease.

Highlights

- Human glial chimeric mice were made using iPSCs derived from schizophrenic subjects
- SCZ glial chimeras develop abnormal astrocytic morphology and hypomyelination
- Differentiation-associated gene expression is impaired in SCZ glial progenitors
- SCZ glial chimeric mice have broad behavioral and sleep abnormalities

Windrem et al., 2017, Cell Stem Cell *21*, 195–208
August 3, 2017
http://dx.doi.org/10.1016/j.stem.2017.06.012

CellPress

Cell Stem Cell
Article

Human iPSC Glial Mouse Chimeras Reveal Glial Contributions to Schizophrenia

Martha S. Windrem,[1] Mikhail Osipovitch,[2] Zhengshan Liu,[1] Janna Bates,[1] Devin Chandler-Militello,[1] Lisa Zou,[1] Jared Munir,[1] Steven Schanz,[1] Katherine McCoy,[1] Robert H. Miller,[4] Su Wang,[1] Maiken Nedergaard,[1,2] Robert L. Findling,[5] Paul J. Tesar,[6] and Steven A. Goldman[1,2,3,7,*]

[1]Department of Neurology and Center for Translational Neuromedicine, University of Rochester Medical Center, Rochester, NY 14642, USA
[2]Center for Neuroscience, University of Copenhagen Faculty of Health and Medical Sciences, 2200 Copenhagen N, Denmark
[3]Neuroscience Center, Rigshospitalet, 2100 Copenhagen, Denmark
[4]Department of Neuroscience, George Washington University School of Medicine, Washington, D.C. 20037, USA
[5]Department of Psychiatry, Johns Hopkins University School of Medicine, Baltimore, MD 21205, USA
[6]Department of Genetics, Case Western University Medical School, Cleveland, OH 44106, USA
[7]Lead Contact
*Correspondence: steven_goldman@urmc.rochester.edu or goldman@sund.ku.dk
http://dx.doi.org/10.1016/j.stem.2017.06.012

SUMMARY

In this study, we investigated whether intrinsic glial dysfunction contributes to the pathogenesis of schizophrenia (SCZ). Our approach was to establish humanized glial chimeric mice using glial progenitor cells (GPCs) produced from induced pluripotent stem cells derived from patients with childhood-onset SCZ. After neonatal implantation into myelin-deficient shiverer mice, SCZ GPCs showed premature migration into the cortex, leading to reduced white matter expansion and hypomyelination relative to controls. The SCZ glial chimeras also showed delayed astrocytic differentiation and abnormal astrocytic morphologies. When established in myelin wild-type hosts, SCZ glial mice showed reduced prepulse inhibition and abnormal behavior, including excessive anxiety, antisocial traits, and disturbed sleep. RNA-seq of cultured SCZ human glial progenitor cells (hGPCs) revealed disrupted glial differentiation-associated and synaptic gene expression, indicating that glial pathology was cell autonomous. Our data therefore suggest a causal role for impaired glial maturation in the development of schizophrenia and provide a humanized model for its in vivo assessment.

INTRODUCTION

Schizophrenia is a uniquely human disorder whose phylogenetic appearance parallels that of glial evolution, which accelerated with the appearance of hominids (Horrobin, 1998; Oberheim et al., 2006, 2009). In particular, astroglial complexity and pleomorphism increased significantly with hominid evolution, which suggests an association between human glial evolution and the development of human-selective neurological disorders, the neuropsychiatric disorders as a case in point. Indeed, a number of both genome-wide association and differential expression studies have highlighted the frequent dysregulation of glia-selective genes, both astrocytic and oligodendrocytic, in schizophrenia (Aberg et al., 2006; Georgieva et al., 2006; Hakak et al., 2001; Hof et al., 2002; Roy et al., 2007; Takahashi et al., 2011; Walsh et al., 2008). At the same time, a number of investigators have highlighted the marked differences between humans and rodents in glial gene expression, in contrast to the relatively conserved nature of neuronal gene expression across mammals (Miller et al., 2010; Sim et al., 2009; Zhang et al., 2016). Together, these studies suggest the correlative association of human glial evolution with the phylogenetic appearance of schizophrenia.

Patients with schizophrenia are typically characterized by a relative paucity of white matter and often frank hypomyelination (Connor et al., 2011; Fields, 2008; Gogtay et al., 2008; McIntosh et al., 2008; Muñoz Maniega et al., 2008; Takahashi et al., 2011), and a number of both pathological and neuroimaging studies have highlighted deficiencies in both oligodendroglial density and myelin structure in affected patients (Fields, 2008; Langmead and Salzberg, 2012; Rapoport et al., 2005; Xia et al., 2016), including at the ultrastructural level (Pruitt et al., 2007; Uranova et al., 2007, 2011). Furthermore, recent studies have emphasized the role of oligodendrocytes in the metabolic support of neurons, suggesting myelin-independent mechanisms whereby oligodendrocytic dysfunction might yield neuronal pathology (Lee et al., 2012; Simons and Nave, 2015). However, despite compelling genetic, cellular, pathological, and radiological studies that have correlated glial and myelin pathology with schizophrenia, many have assumed that clinical hypomyelination among schizophrenics is secondary to neuronal pathology, so the contribution of cell-autonomous glial dysfunction to schizophrenia has not been well studied.

This lapse has in large part been due to the lack of animal models of human glial pathophysiology: mouse brains have mouse glia. We therefore asked whether this limitation might be addressed using a novel model of human glial chimeric mice (Goldman et al., 2015; Han et al., 2013; Windrem et al., 2008) paired with the development of protocols for generating bipotential astrocyte-oligodendrocyte glial progenitor cells (GPCs) from patient-specific human induced pluripotent stem cells (hiPSCs) (Wang et al., 2013). In these human glial chimeric mouse brains, the majority of resident glia are replaced by

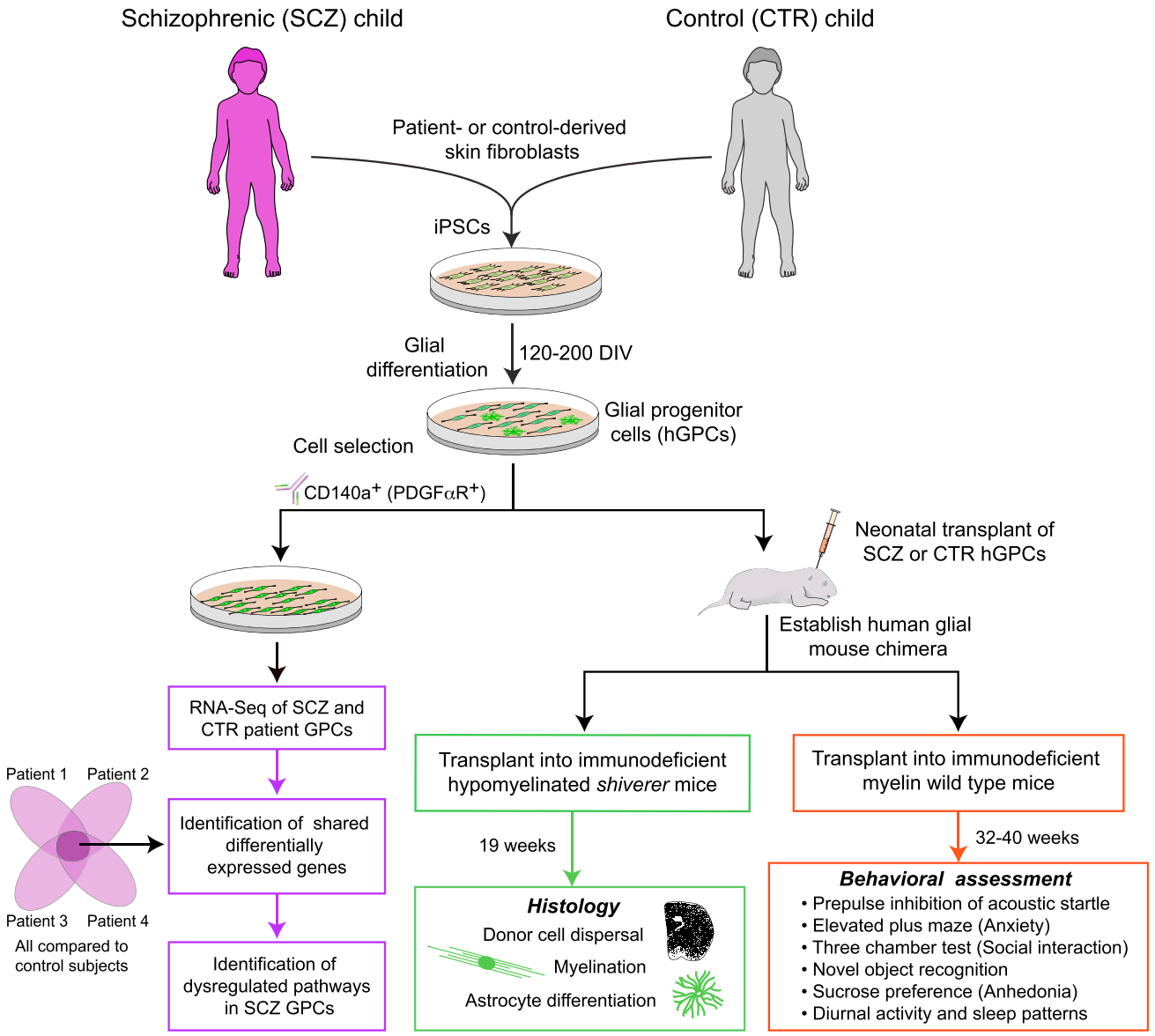

Figure 1. Functional and Genomic Assessment of SCZ-Derived Glial Progenitor Cells

This schematic summarizes the steps involved in our analysis of glial progenitor cells derived from individuals with juvenile-onset SCZ compared with GPCs derived from behaviorally normal controls. The major output data include effects of SCZ origin on in vivo oligodendrocyte maturation and myelination (Figure 2), in vivo astrocyte differentiation and phenotype (Figure 3), in vitro differential gene expression (Figures 4 and 5), and behavioral phenotype of the human glial chimeric host animals (Figure 6).

See also Figure S1 and Table S1.

human glia and their progenitors (Windrem et al., 2014), allowing human glial physiology, gene expression, and effects on neurophysiological function to be assessed in vivo, in live adult mice (Han et al., 2013). In this study, we used this glial chimeric model to assess the contribution of human glia to the schizophrenic disease phenotype. To this end, we prepared human glial progenitor cells (hGPCs) from iPSCs derived from fibroblasts taken from either juvenile-onset patients with schizophrenia (SCZ) or their normal controls, assessed the differential gene expression of SCZ hGPCs relative to those of normal subjects, and transplanted these cells into immunodeficient neonatal mice to produce patient-specific human glial chimeric mice. The glial chimeric mice were then analyzed regarding the effects of SCZ derivation on astrocytic and oligodendrocytic differentiation in vivo as well as for behavioral phenotype, and the data thereby obtained correlated to disease-associated gene expression (Figure 1).

RESULTS

Patients with juvenile-onset SCZ as well as healthy young adult controls free of known mental illness were recruited, and skin

biopsies were obtained from each. Patient identifiers were not available to investigators besides the treating psychiatrist, although age, gender, race, diagnosis, and medication history accompanied cell line identifiers. Fibroblasts were isolated from each sample; from these, 11 new independent hiPSC lines were derived from eight patient samples (five juvenile-onset SCZ patients and three healthy gender-matched and age-analogous controls (Table S1). iPSCs were generated using the excisable floxed polycistronic hSTEMCCA lentivirus (Somers et al., 2010; Zou et al., 2012) encoding Oct4, Sox2, Klf4, and c-Myc (Takahashi et al., 2007; Welstead et al., 2008). All lines were initially characterized and validated as pluripotent using global transcriptome profiling by RNA sequencing to assess pluripotent gene expression as well as immunostaining for Oct4, Nanog, and SSEA4. The identity of each iPSC line was confirmed to match the parental donor fibroblasts using short tandem repeat (STR)-based DNA fingerprinting. iPSC line isolates were also karyotyped concurrently with these experiments to confirm genomic integrity. An additional well-characterized hiPSC control line, C27 (Chambers et al., 2009), was used to ensure that our control engraftment and differentiation data were consistent with prior studies in our lab (Wang et al., 2013). Altogether, we evaluated hGPC preparations from seven iPSC lines derived from five SCZ patients and five iPSC lines derived from four control subjects (Table S1). We instructed these iPSC cells to a GPC fate as described previously (Wang et al., 2013) and, after $\geq$105 days in vitro (DIV) under glial differentiation conditions, validated the predominant GPC phenotype of each cell population using flow cytometry for CD140a/PDGFαR (platelet-derived growth factor receptor alpha) (Figure S1; Sim et al., 2011). To optimize glial differentiation in vivo, we limited transplants to preparations in which most cells were CD140a$^+$ GPCs, with the remainder astroglial.

We first asked whether SCZ hGPCs differed from wild-type hGPCs in their myelination competence. To this end, we implanted SCZ hGPCs into neonatal immunodeficient shiverer mice (rag2$^{-/-}$ × MBP$^{shi/shi}$), a congenitally hypomyelinated mutant lacking myelin basic protein (MBP) (Roach et al., 1983; Rosenbluth, 1980). As these otherwise myelin-deficient mice matured, their engrafted hGPCs differentiated into both astrocytes and myelinogenic oligodendrocytes, yielding mice chimeric for individual patient-derived glia (Windrem et al., 2008, 2014). By this means, we established mice with patient-specific, largely humanized forebrain white matter derived from SCZ or control subjects (Figures 2A–2D).

SCZ Glial Chimeric Mice Were Uniformly Hypomyelinated

We first noted that the SCZ hGPCs manifested an aberrant pattern of migration upon neonatal transplantation. Normal control hGPCs invariably expanded through the white matter before colonizing the cortical gray matter (Figure 2A), as we have noted previously in both fetal tissue- and hiPSC GPC-engrafted shiverer mice (Wang et al., 2013; Windrem et al., 2008). In contrast, SCZ GPCs preferentially migrated earlier into the gray matter in shiverer mice, with large numbers traversing without stopping in the callosal white matter (n = 4 lines from 4 different patients, each with $\geq$3 mice/patient, each versus paired controls) (Figure 2B; Figure S2). This resulted in significantly fewer donor hGPCs in the white matter of shiverers engrafted with SCZ GPCs (Figures 2H and 2I; Figure S2). Importantly, this was associated with substantially diminished central myelination in these mice, as reflected by both MBP immunostaining (Figures 2C–2F) and myelin luminance (Figure 2G).

Because the SCZ hGPC-engrafted shiverers manifested deficient myelination, we asked whether this was due to a relative failure of SCZ hGPCs to remain within white matter or, rather, due to a cell-intrinsic failure in myelinogenesis. Examining 19-week-old SCZ and control hGPC-engrafted shiverer mice, we found significantly fewer human nuclear antigen (hNA)-defined, donor-derived cells in SCZ hGPC-engrafted shiverer white matter (40,615 ± 2,189 × 10^3 hNA$^+$ cells/mm^3, n = 18) than in mice identically transplanted with control hGPCs (69,970 ± 4,091/mm^3, n = 32, $p < 0.0001$ by two-tailed t test; Fagerland and Sandvik, 2009; Zimmerman, 2004) (Figure 2H). Moreover, the numbers of hNA$^+$ donor cells co-expressing the oligodendroglial lineage marker Olig2 were similarly depressed in SCZ hGPC-engrafted mice (33,619 ± 2,435/mm^3, n = 26) relative to control hGPC-engrafted mice (46,139 ± 2,858/mm^3, n = 17, $p < 0.002$ by two-tailed t test) (Figure 2I). On that basis, we next found that the density of transferrin-defined human oligodendroglia was similarly lower in the callosal white matter of SCZ hGPC chimeras than in control hGPC chimeras (8,778 ± 892.2/mm^3, n = 25 versus 17,754 ± 2,023/mm^3, n = 17, respectively; $p = 0.0006$ by two-tailed t test) (Figure 2J). These data indicate that SCZ GPCs are deficient not only in their colonization of the forebrain white matter but also in their oligodendrocytic differentiation, with a resultant suppression of central myelinogenesis. Together, these findings suggest that SCZ hGPCs migrate aberrantly, traversing rather than homing to developing white matter, thus yielding relatively poor white matter engraftment, deficient myelin formation, and premature cortical entry relative to normal GPCs.

SCZ Glial Chimeric Mice Manifested Developmentally Delayed Astrocytic Maturation

We next asked whether the SCZ hGPCs that prematurely entered the gray matter differentiated instead into astrocytes in that environment or whether they rather manifested an impairment in lineage progression that prevented their astrocytic differentiation as well. Both SCZ- and control hGPC-engrafted shiverer brains were immunostained for astrocytic glial fibrillary acidic protein (GFAP) 19 weeks after neonatal graft using a species-specific anti-human GFAP antibody. We found that astrocytic maturation from engrafted hGPCs was markedly deficient in the SCZ hGPC-engrafted brains (n = 19, derived from 3 SCZ patient lines, and n = 12 control mice, from 3 control patients) (Figures 3A and 3B). In the callosal white matter as well as in both the striatal and cortical gray matter, astrocytic differentiation by SCZ hGPCs was significantly less than that of control GPCs so that, although all control hGPC forebrains showed dense human GFAP$^+$ astrocytic maturation, far fewer SCZ hGPCs manifested hGFAP expression and an astrocytic phenotype (controls: 6,616 ± 672.3 GFAP$^+$ cells/mm^3 in callosum, n = 12; SCZ: 1,177 ± 276.6 GFAP$^+$ callosal cells/mm^3, n = 19; $p < 0.0001$ by two-tailed t test; Figure 3C). This defect in astrocytic differentiation was consistently observed in all mice (n = 19) derived from the three SCZ patients assessed compared with the control GPC-engrafted mice (n = 12) derived

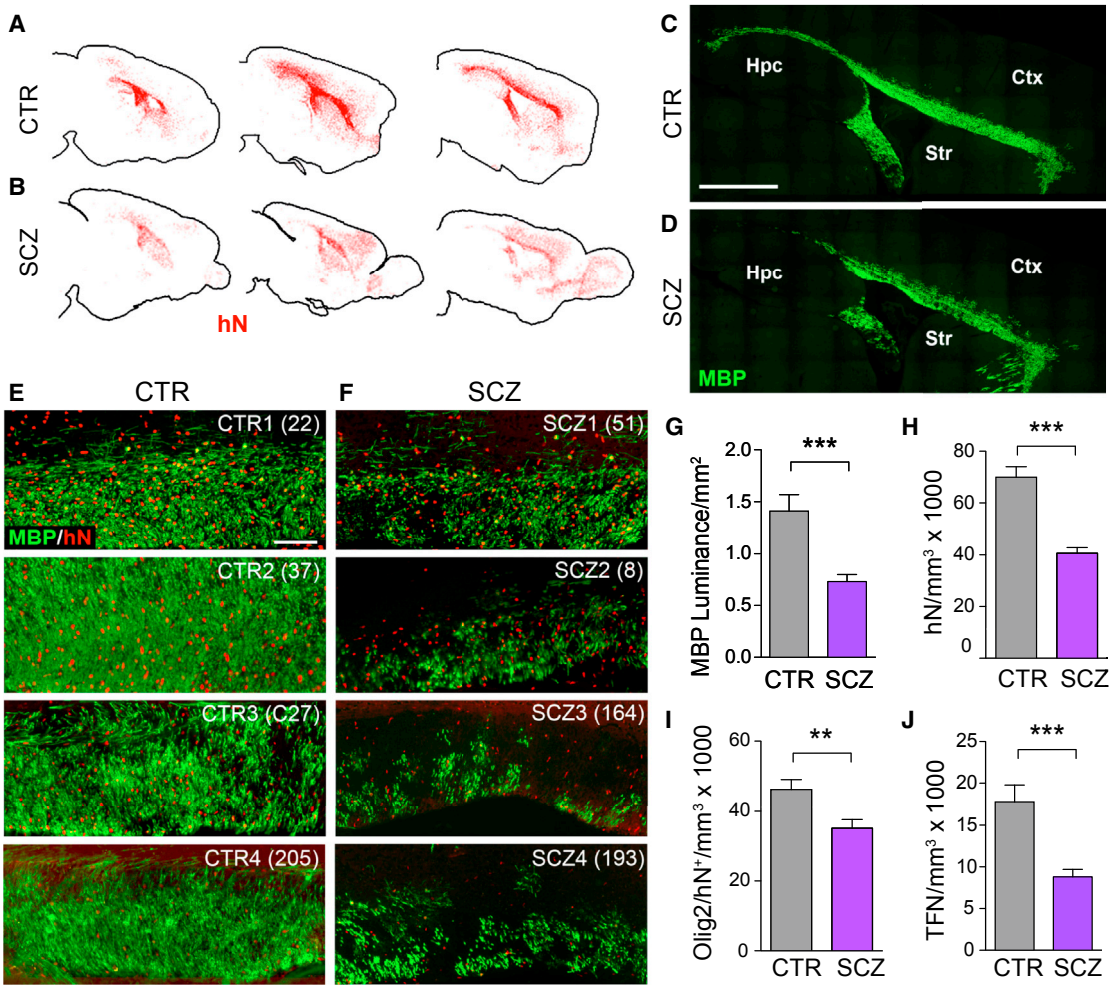

Figure 2. SCZ-Derived hGPCs Exhibit Aberrant Dispersal and Relative Hypomyelination

Human iPSC GPC chimeras were established by neonatal hGPC injection into shiverer hosts and sacrificed at 19 weeks.

(A and B) GPCs derived from a control subject (A) dispersed primarily in the major white matter tracts, whereas SCZ-derived GPCs (B, 15-year-old male) showed less white matter residence and more rapid cortical infiltration.

(C and D) Sagittal sections reveal that callosal myelination by SCZ GPCs (D) was less dense than that by control hGPCs (C).

(E and F) Higher-power images from chimeric mice engrafted with hGPCs from four control patients (E) versus chimeric mice engrafted with hGPCs from four different SCZ patients (F).

(G) MBP luminance confirmed the greater callosal myelination of CTRL GPC-engrafted versus SCZ GPC-engrafted mice at 19 weeks (means of four different SCZ and CTRL patients each, $n \geq 3$ mice/patient) ($p = 0.0002$, t test).

(H–J) Absolute donor cell densities were lower in SCZ- than control hGPC-engrafted corpus callosum (H, $p < 0.0001$, t test), as were the densities of olig2$^+$ hGPCs and oligodendroglia (I, $p = 0.002$, t test) and transferrin (TFN)$^+$ oligodendroglia (J, $p < 0.0001$, t test).

$^{**}p < 0.002$ (I); $^{***}p < 0.0001$ (H, J) or <0.0002 (G). In (C) and (D), the figures are derived from individual higher power photos taken in the X-Y plane, then stitched together as wide-field montages in StereoInvestigator. See also Figure S2.

from three normal subjects (Figure 3D) and reflected in part the lower proportion of GFAP$^+$ astrocytes that developed among engrafted human cells in the SCZ HGPC-engrafted brains (Figure 3E). Furthermore, Sholl analysis of individual astroglial morphologies (Sholl, 1953), as imaged in 150-μm sections and reconstructed in Neurolucida (Figure 3J), revealed that astrocytes in SCZ hGPC chimeras differed significantly from their control hGPC-derived counterparts, with fewer primary processes (Figure 3F), less proximal branching (Figure 3G), longer distal fibers (Figure 3H), and less coherent domain structure (Figure 3I). Thus, SCZ hGPCs derived from multiple patients exhibited a common defect in phenotypic maturation and, hence, proved to be deficient in astrocytic differentiation as well as myelination.

SCZ hGPCs Showed Cell-Autonomous Misexpression of Differentiation-Associated Genes

To better define the molecular basis for the apparent impediment to terminal glial differentiation in SCZ GPC-engrafted mice and to define which aspects of that deficit might be cell-autonomous, we next used RNA sequencing (RNA-seq) analysis to identify the differentially expressed genes of SCZ iPSC-derived GPCs relative to those of control-derived glia. We used sequencing data to reconstruct the transcriptional

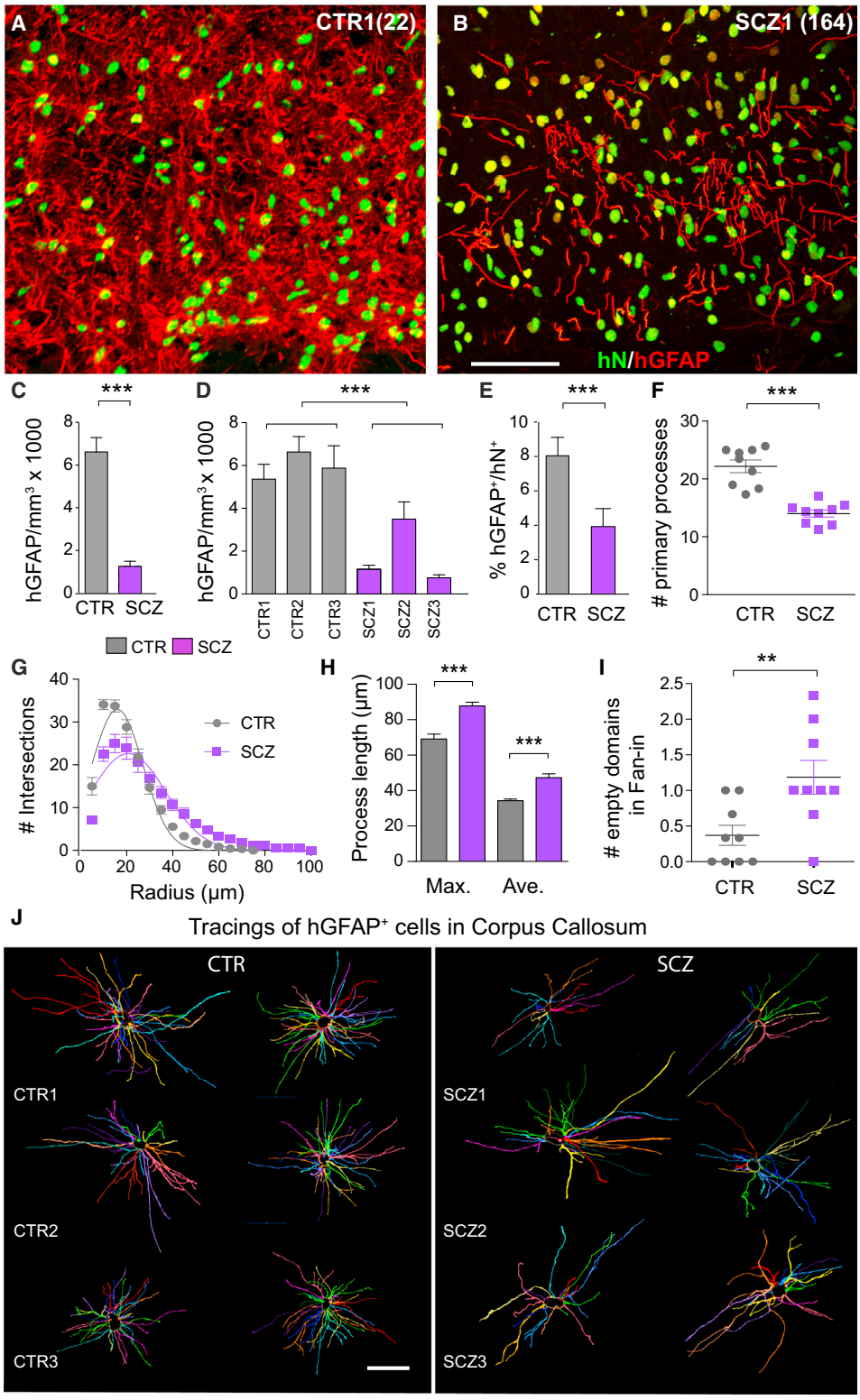

Figure 3. Astrocytic Differentiation Is Impaired in SCZ hGPC Chimeric Brain

Human iPSC GPC chimeras were established in immunodeficient shiverer hosts and sacrificed at 19 weeks, and astrocytic differentiation was assessed. (A and B) Representative images of the corpus callosum of mice neonatally injected with iPSC GPCs derived from either control (A, line 22) or schizophrenic (B, line 164) subjects (human nuclear antigen, green; glial fibrillary acidic protein, red). Control hiPSC GPCs from all tested patients rapidly differentiated as GFAP$^+$ astrocytes, with dense fiber arrays in both callosal white and cortical gray matter (A). In contrast, SCZ GPCs were slow to develop mature GFAP expression (B).

(legend continued on next page)

patterns of hGPCs derived from four different SCZ and three control patients. hGPCs were derived at time points ranging from 154–242 days in vitro and sorted for hGPCs using CD140a-targeted fluorescence-activated cell sorting (FACS). Using a 5% false discovery rate (FDR) and a fold change threshold of 2, we identified a total of 116 mRNAs that were differentially expressed by CD140a-sorted SCZ hGPCs relative to their control iPSC hGPCs (Figures 4A and 4B). Among the genes most differentially expressed by CD140a-sorted SCZ hGPCs were a host of glial differentiation-associated genes, in particular those associated with early oligodendroglial and astroglial lineage progression, which were uniformly downregulated in the SCZ hGPCs relative to their normal controls (Figures 4C and 4F). These included a coherent set of the key GPC lineage transcription factors OLIG1, OLIG2, SOX10, and ZNF488 as well as genes encoding stage-regulated proteins involved in myelination, such as GPR17, UGT8, OMG, and FA2H (Figure 4G; see Table S2 and Figures S3 and S4 for detailed gene expression data).

These expression data suggest that the diminished myelination of SCZ hGPC-transplanted shiverer brains reflected aberrant oligodendrocytic differentiation from the engrafted SCZ hGPCs. Similarly, because hGPCs give rise to astrocytes as well as oligodendrocytes, the RNA expression data suggest an analogous impediment to astrocytic differentiation. The functional consequences of the latter are especially profound, given the critical role of astrocytes in synaptic development and function; indeed, the relative suppression of astrocytic differentiation by SCZ hGPCs suggests a glial contribution to the impaired synaptic function noted in SCZ. In that regard, further functional analysis of SCZ-associated dysregulated hGPC genes identified channel and receptor activity as well as synaptic transmission as the most differentially affected functions besides glial differentiation (Figures 4D and 4E). These disease-linked channel and synapse-associated genes were largely downregulated in SCZ hGPCs and included a number of potassium channel genes (Figure 4D), including KCND2, KCNJ9, KCNK9, and KCNA3, as well as a number of transcripts associated with synaptic development and function (Figure 4E; Table S2). The latter included NXPH1, NLGN3, and LINGO1, among others (Table S3; Figures S3 and S4), synaptic genes whose dysregulation has been previously linked to both SCZ and autism spectrum disorders (Andrews and Fernandez-Enright, 2015; Fernandez-Enright et al., 2014; Maćkowiak et al., 2014; Salyakina et al., 2011; Südhof, 2008). Although the expression of these latter genes was suppressed in hGPCs derived from all four SCZ patients, other synapse-associated genes, such as NRXN1, NLGN1, DSCAML1, and the SLITRKs 2–5, were sharply downregulated in hGPCs derived from three of the four patients but not in the fourth (Table S3). However, other synapse-associated transcripts, like NXPH3 and NTRNG2, were similarly downregulated in some patients but not others. TaqMan low-density arrays were used for quantitative real-time PCR validation of these and other dysregulated transcripts of interest and confirmed the significant differential downregulation of these differentiation- and synaptic function-associated genes (Figure 5).

Together, these data suggest the importance of glia-associated synaptic gene expression in SCZ and emphasize the heterogeneity of pathways that might be mechanistically complicit in its dysregulation. These data also highlight the point that, although the neuronal localization of these synaptic proteins has long been recognized, their synthesis by glia and the synaptic contributions thereof have not been specifically discussed, although cell-type-specific transcriptional databases have noted significant glial expression of these genes (Zhang et al., 2014). Because NRXN1, a synapse-associated transcript closely linked to SCZ (Südhof, 2008), was one of the most strongly and consistently downregulated glial genes across our patients, we verified the downregulation of its expression by SCZ glia by immunoblotting CD140a-sorted, neuron-free isolates of SCZ and control hGPCs. Western blots revealed that neurexin-1 was indeed abundantly expressed by human GPCs and that neurexin-1 protein levels were sharply lower in otherwise matched SCZ hGPCs (Figure S5).

SCZ Glial Chimerization Yielded a Disease-Specific Behavioral Phenotype

We next asked whether the alterations in glial distribution and differentiation observed in mice engrafted with SCZ hGPCs might alter the behavioral phenotype of the host mice. In particular, we postulated that the aberrant infiltration of hGPCs and their derived astroglia into the developing cortex might influence information processing within the cortex when mature. As noted, past studies have reported both the influence of astrocytic networks on synaptic efficacy and plasticity and the differential competence of hominid glia in this respect (Han et al., 2013; Oberheim et al., 2009). Human glial chimeric mice manifest a lower threshold for hippocampal long-term potentiation (LTP) and learn more rapidly, with superior performance in a variety of learning tasks that include auditory fear conditioning, novel object and place recognition, and Barnes maze navigation. In each of these tests, but not in any test of social interactivity or primary perception, human glial chimeras acquire new causal associations more quickly than allografted or untransplanted controls (Han et al., 2013). Thus, engrafted human GPCs and their daughter glia can integrate into, and substantially modify, developing neural networks (Franklin and Bussey, 2013). On

(C–E) At 19 weeks, GFAP$^+$ astrocyte densities were significantly greater in mice chimerized with control than SCZ-derived GPCs, both as a group (C) and when analyzed line by line (D). This was not just a function of less callosal engraftment because the proportion of human donor cells that developed GFAP and an astrocytic phenotype was significantly lower in SCZ- than control GPC-engrafted mice (E).

(F–J) Sholl analysis of individual astroglial morphologies (Sholl, 1953), as imaged in 150-μm sections and reconstructed in 3D by Neurolucida (J), revealed that astrocytes in SCZ hGPC chimeras differed significantly from their control hGPC-derived counterparts, with fewer primary processes (F), less proximal branching (G), and longer distal fibers (H). When the 3D tracings (J) were assessed by Fan-in radial analysis (MBF Biosciences; Dang et al., 2014), an approach by which 3D fiber distributions are quantified as to radial segments occupied, control astrocytic processes were noted to extend uniformly in all directions, whereas SCZ astrocytic processes left empty spaces, indicative of a discontiguous domain structure (I).

***$p < 0.0001$ by t test (C, E, F, and H) and by two-way ANOVA (D); **$p < 0.002$ (I); $p < 0.0001$ by non-linear comparison (G). Scale bars, 50 μm (A and B) and 25 μm (J).

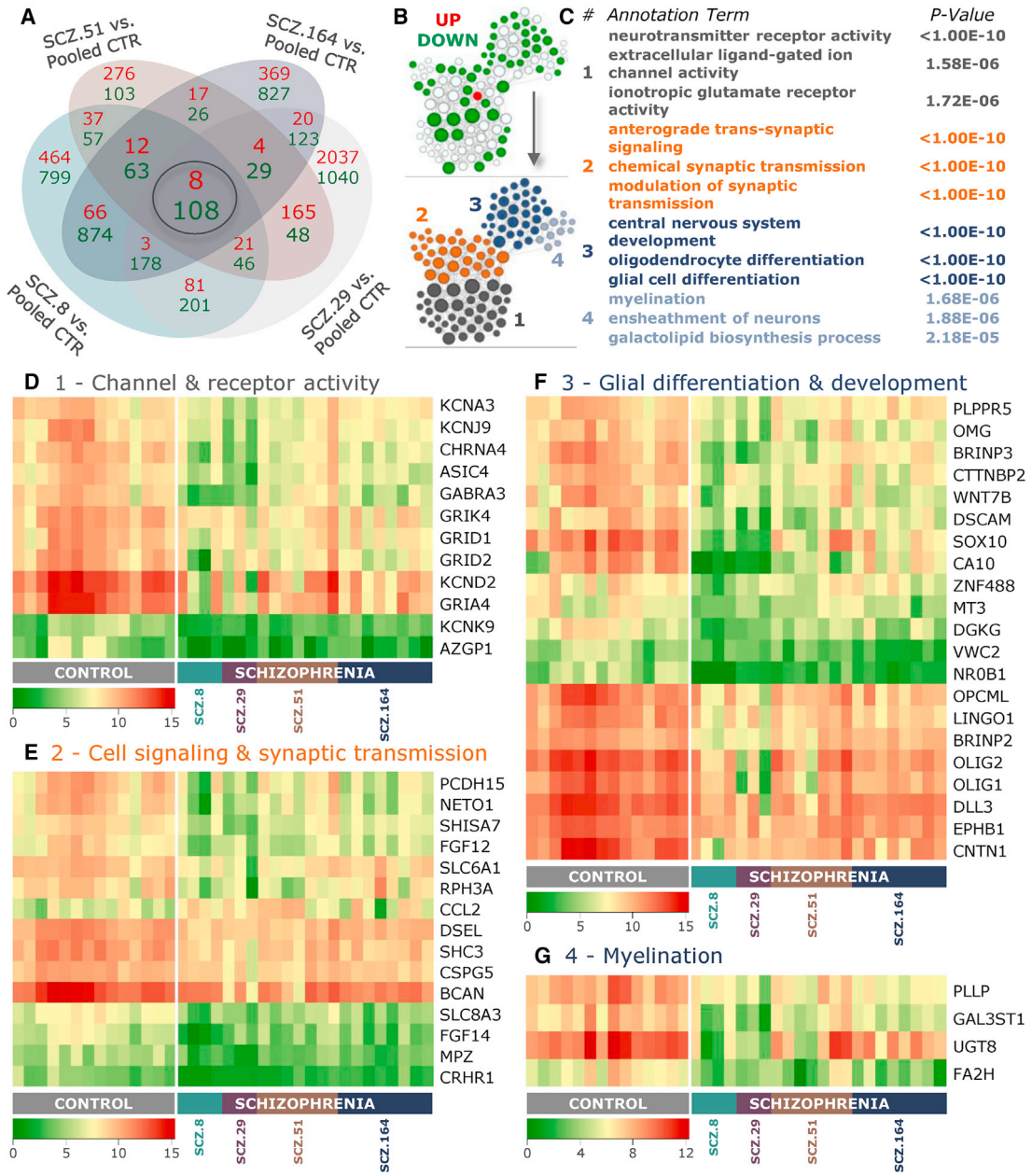

Figure 4. SCZ-Derived hGPCs Suppress Glial Differentiation-Associated Gene Expression

RNA sequence analysis reveals differential gene expression by SCZ hGPCs.

(A) Intersection of lists of differentially expressed genes (DEGs) (log2 fold change > 1.00, FDR 5%) obtained by comparison of hGPCs derived from four different SCZ patients compared with pooled control hGPCs.

(B) Network representation of functional annotations for the intersection gene list shown in (A). In the top network, green and red nodes represent down- and upregulated genes, respectively, and white nodes represent significantly associated annotation terms (FDR-corrected $p < 0.01$; annotation terms include Gene Ontology: Biological Process (GO:BP), Gene Ontology: Molecular Function (GO:MF), pathways, and gene families, and nodes are sized by degree). The bottom network highlights four highly interconnected modules identified by community detection.

(C) Top annotation terms identified for each module in (B).

(D) Heatmap representation of 12 conserved DEGs that are associated with module 1 (gray in B, 32.4%), which includes annotations related to neurotransmitter receptor and gated channel activity.

(E) Heatmap representation of 15 conserved DEGs associated with module 2 (orange in B, 28.7%), which comprises annotations related to cell-to-cell signaling and synaptic transmission.

(F) Heatmap representation of 21 conserved DEGs associated with module 3 (dark blue in B, 28.7%), including annotations related to CNS and glial differentiation.

(G) Heatmap representation of four conserved DEGs that are associated with module 4 (light blue in B, 10.2%), with annotations related to myelination and lipid biosynthesis. The absolute expression in heatmaps is shown in UQ-normalized, log2-transformed counts (Li et al., 2015).

See also Figures S3 and S4 and Table S2.

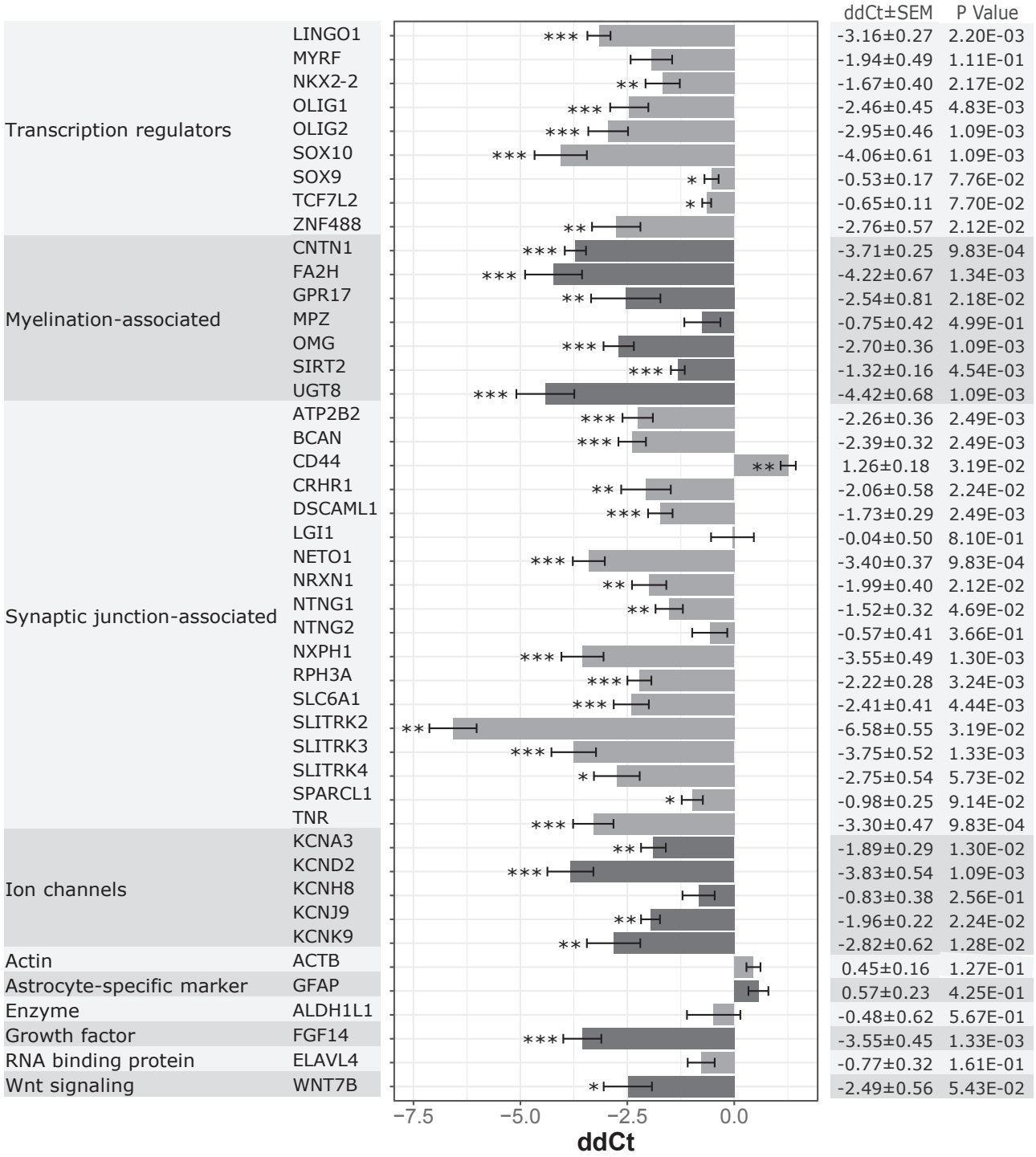

Figure 5. Impaired Glial Differentiation-Associated Gene Expression by SCZ hGPCs

The expression of dysregulated genes in SCZ-derived GPCs, as identified by RNA-seq analysis, was assessed by TaqMan low-density array (TLDA) qRT-PCR and then compared with that of control hGPCs. Expression data were normalized to the GAPDH endogenous control. Mean delta delta Ct (ddCt) values and SE ranges, calculated from four pooled SCZ GPC lines (n = 19) that were individually compared with three pooled control GPC lines (n = 10), are shown. The difference in gene expression by SCZ and control hGPCs was assessed by paired t tests, followed by multiple testing correction by Benjamini-Hochberg (BH) procedure (***$p < 0.01$, **$p < 0.05$, *$p < 0.1$). 48 genes were assessed. 45 genes are shown, excluding the endogenous control and genes that had high proportions of undetermined or unreliable reactions, LRFN1 and NEUROD6. The vast majority of genes were confirmed as dysregulated in SCZ-derived GPCs. Analysis of TLDA data was performed in ExpressionSuite software version 1.1, supplied by Applied Biosciences.

See also Table S3.

that basis, we postulated that the disruption in normal glial development noted in our SCZ glial chimeras might yield disease-associated changes in learning and behavior. To address this question, we assessed the behavioral phenotypes of immunodeficient but otherwise wild-type mice neonatally engrafted with SCZ GPCs relative to matched hosts engrafted with control-derived GPCs. For these experiments, we used normally myelinated hosts rather than shiverer mice to produce mice chimeric only for human GPCs and astrocytes and not for oligodendroglia, thus isolating any observed behavioral effects to SCZ hGPCs and astrocytes.

We first asked whether schizophrenic derivation of engrafted glia affected prepulse inhibition (PPI), a behavioral hallmark of both clinical schizophrenics and animal models thereof (Ewing and Grace, 2013). PPI reflects the coordination of sensorimotor gating in the CNS, and its diminution may predict aspects of a schizophrenic phenotype (Ivleva et al., 2014; Kohl et al., 2013). We found that, when assessed at 6 months of age, the latest time point at which the C57BL/6 background strain of our rag1$^{-/-}$ mice can be reliably assessed (because these mice suffer premature auditory loss that might otherwise diminish auditory PPI), that mice engrafted with SCZ hGPCs exhibited significantly diminished auditory prepulse inhibition (Figure 6A) and did so at all volumes of prepulse. Given the strong effect of SCZ glial chimerization on PPI, we next asked whether SCZ glial chimerization might be associated with changes in behavior in cognitive and socialization tests. To that end, we compared SCZ and control chimeras in a battery of behavioral tests that included the elevated plus maze, a measure of anxiety (Walf and Frye, 2007); the three-chamber social challenge (Yang et al., 2011); novel object recognition, a focused measure of executive memory (Bevins and Besheer, 2006); and the preference for sucrose water, a test for anhedonia (Barnes et al., 2014; Willner et al., 1987). In each, mice chimerized with one of three SCZ or three control patient-derived lines were compared; each line was derived from a different patient. Between 6–12 recipient mice were engrafted and tested per cell line, or 17–36 mice per group for each behavioral comparison, with a typically equal balance of male and female recipients. These animals were tested beginning between 30–36 weeks of age, and testing typically lasted 3 weeks. Over the tested age range, the SCZ GPC chimeric mice exhibited a number of significant differences in behavior relative to their control hGPC-engrafted counterparts. SCZ hGPC mice exhibited greater avoidance of the open arms in the elevated plus maze than the normal hGPC-engrafted controls ($n = 36$ mice/group, each including 12 mice engrafted with hGPCs from each of three patients; $p = 0.036$, two-tailed t test), suggesting that the SCZ hGPC mice were prone to higher anxiety when challenged (Figure 6B). In addition, the SCZ hGPC mice showed less preference for sucrose water, consistent with relative anhedonia (Figure 6C), less interest in strange mice in the three-chamber social test (Figure 6D), and relatively poor novel object recognition (Figure 6E), reflecting relative impairment in executive memory.

As an additional metric of SCZ-associated behavior, we then assessed sleep and diurnal activity patterns of human SCZ and CTRL glial chimeras, directly comparing mice engrafted with either SCZ (line 52) or control (line 22) hGPCs. We found that mice engrafted with SCZ GPCs were significantly more active than control mice engrafted with normal hGPCs. As measured by meters moved per hour, over the course of a 72-hr video recording (Noldus Ethovision), the SCZ hGPC chimeric mice moved significantly more than their normal hGPC-engrafted controls (two-way ANOVA, $F = 48.35$, $p < 0.0001$) (Figure 6F). Interestingly, although the SCZ-associated increment in activity largely occurred during nighttime periods of wakefulness, the SCZ mice also manifested disrupted sleep patterns, as measured by the duration of bouts of inactivity, a surrogate for electroencephalogram (EEG)-validated sleep (McShane et al., 2010; Pack et al., 2007; Figure 6G). Within the half hour following the phase transition from dark to light (when mice normally sleep), the control (CTRL) mice had more continuous, uninterrupted patterns of sleep, with an average sleep bout of 511.5 ± 36.4 s (8.53 min), whereas SCZ mice were asleep for 306.2 ± 43.7 s, or 5.1 min per bout ($p < 0.01$ by two-way ANOVA, with Bonferroni post hoc t tests). The shorter average periods of inactivity manifested by SCZ hGPC mice during the normal daytime transition to sleep suggest that SCZ hGPC chimerization disrupted normal daytime sleep patterns while increasing nighttime activity. Together, these results suggest that SCZ glial chimerization was sufficient to yield heightened anxiety and fear in engrafted recipients as well as disease-associated deficits in socialization, cognition, and sleep patterning, all features associated with human SCZ.

DISCUSSION

These data suggest a significant contribution of cell-autonomous glial pathology to the genesis and development of juvenile-onset SCZ. In these human glial chimeric mice, SCZ-derived iPSC hGPCs exhibited aberrant migration with deficient engraftment in the central white matter relative to age-analogous and gender-matched control iPSC hGPCs. Although a fraction of SCZ hGPCs that did remain within the white matter differentiated as normal myelinogenic oligodendroglia, the premature cortical influx and, hence, lower density of donor-derived cells in the white matter of SCZ hGPC-engrafted mice resulted in the latter's overt hypomyelination relative to mice engrafted with control GPCs. Thus, SCZ hGPCs appeared to traverse, rather than home in on, the nascent white matter, resulting in sparse hGPC colonization and, hence, deficient forebrain myelination. The aberrant dispersal pattern of SCZ hGPCs suggests that SCZ GPCs may not recognize developmental stop signals that permit progenitors to dwell and expand within the presumptive white matter before colonizing the cortical mantle and may, instead, be biased toward rapid entry into the cortical gray matter. These observations in human SCZ glial chimeric mice are especially intriguing given the well-described hypomyelination of schizophrenic patients (Davis et al., 2003; Najjar and Pearlman, 2015; Sigmundsson et al., 2001; Voineskos et al., 2013), particularly so in early-onset disease (Gogtay et al., 2008; Gogtay and Rapoport, 2008; Samartzis et al., 2014).

These anatomic observations were especially notable in light of the differential gene expression pattern of the SCZ hGPCs, which revealed that the cells were deficient not only in early glial differentiation-associated transcripts but also in genes that encode for synaptic proteins typically associated with transducing activity-dependent signals (Südhof, 2008). Together,

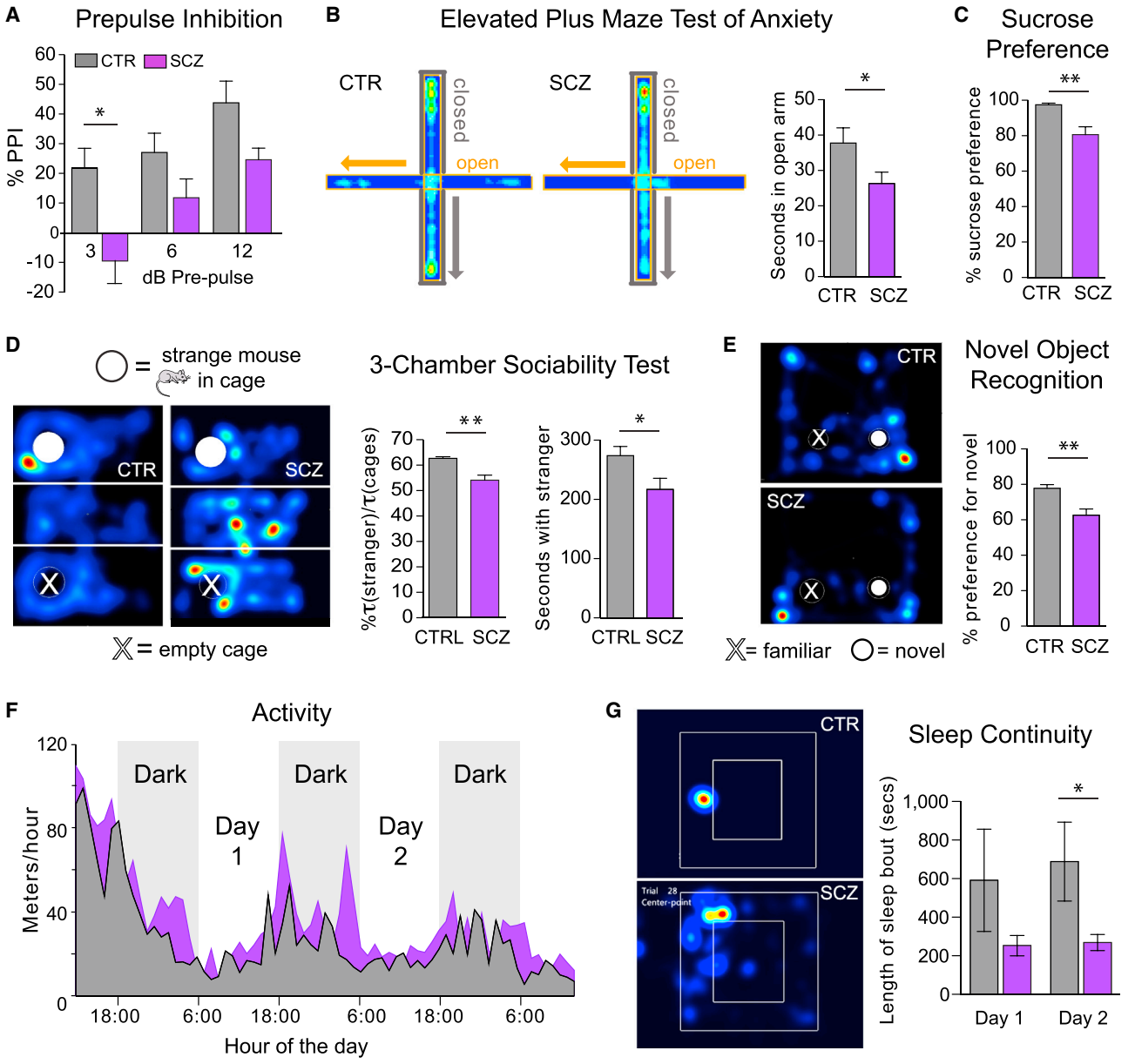

Figure 6. SCZ-Derived Human Glial Chimeras Have Significant Behavioral Abnormalities

(A–E) Behavioral tests were performed in mice chimerized with one of three SCZ or three control hGPC lines, each line from a different patient. 7–20 recipient mice were tested per cell line, males and females equally.

(A) Prepulse inhibition normally myelinated rag1$^{-/-}$ mice engrafted with SCZ hGPCs had reduced auditory prepulse inhibition (PPI) at all volumes of prepulse. The extent of PPI differed significantly between control (n = 13) and SCZ (n = 27) hGPC-engrafted animals (p = 0.0008 by ANOVA, F = 11.76 [1,114]).

(B) Elevated plus maze. Left: representative heatmaps of the cumulated movement of a mouse engrafted with SCZ hGPCs, relative to its matched normal hGPC-engrafted control, in the elevated plus maze, a test designed to assess anxiety, in which preference for enclosed space and avoidance of open height suggests greater anxiety. Right: mice engrafted with hGPCs from three SCZ patients (12 implanted mice each for n = 36 mice total) spent more time in the closed maze arms than control-engrafted mice (n = 36, also derived from three patients) (p = 0.036, two-tailed t test).

(C) Sucrose preference. SCZ GPC-engrafted mice were less likely to prefer sweetened water, suggesting relative anhedonia (p = 0.02, Mann-Whitney t test; n = 30 mice derived from three SCZ lines; n = 17 mice from three control lines).

(D) Three-chamber socialization test. Mice engrafted with hGPCs were placed into the middle chamber of a box divided into three compartments, one holding an empty cage (bottom, X) and one containing an unfamiliar mouse (top, filled white circle) and then video-tracked for 10 min. Mice engrafted with SCZ hGPCs (right heat-map) avoided strangers more than control mice (left heatmap), spending less time with strangers, whether analyzed as the proportion of time spent with the strange mouse relative to the empty cage (left bar graph, p = 0.005) or the net amount of time spent with the strange mouse (right bar graph, p = 0.02); three SCZ lines, 39 mice; four control lines, 52 mice).

(E) Novel object recognition. Mice engrafted with SCZ hGPCs showed significantly poorer novel object recognition (p = 0.0006; three SCZ lines, 19 mice; three control lines, 28 mice).

(legend continued on next page)

these anatomic and transcriptional data suggest that SCZ hiPSC-derived GPCs might be subject to impaired phenotypic differentiation, which might result in their neglect of the local neuronal signals that typically regulate the expansion and maturation of GPCs (Barres and Raff, 1993); this might account for their rapid transit through the white matter into the overlying cortex and, hence, the diminished callosal GPC density and hypomyelination of SCZ chimeric shiverer mice (Figure 2). Thus, the myelination defect in SCZ hGPC chimeras appeared because of both deficient oligodendrocytic differentiation and the relative dearth of SCZ hGPCs remaining within the white matter. Moreover, astrocytic differentiation from SCZ hGPCs was also impaired and may have contributed further to hypomyelination in the SCZ glial chimeras, given the metabolic dependence of mature oligodendrocytes on local astrocytes (Amaral et al., 2013; John, 2012).

Importantly, the defective astrocytic maturation of SCZ hGPCs might also have profound effects on developmental synaptogenesis and circuit formation as well as on myelinogenesis. Neural connectivity and synaptic development are both intimately dependent on astrocytic guidance (Clarke and Barres, 2013; Ullian et al., 2001) and, hence, on the appropriate timing of astrocytic appearance and maturation. As a result, any disruption in astrocytic maturation by SCZ hGPCs, as observed in each of the SCZ lines we studied, might be expected to significantly confound the construction and functional architecture of neural networks in which SCZ hGPCs are resident. Moreover, glial progenitors themselves may have significant interactions with local neurons (Sakry et al., 2014) so that their dysfunction might disrupt local neuronal response thresholds and circuit formation.

Besides the anatomic observation of deficient astrocytic maturation in SCZ hGPC chimeras, our genomic analysis of SCZ-derived hGPCs revealed significant downregulation in hGPCs derived from all four SCZ patients of a number of synaptic genes, including neuroligin-3, neuroexophilin-1, and LINGO1, relative to their normal controls (Table S3; Figure 5). Other synapse-associated genes, such as neurexin-1 and DSCAML1, were significantly and sharply downregulated in GPCs derived from three patients (lines 8, 29, and 51) but not in the fourth (line 164). Similarly, SLITRKs 2–5 were significantly and sharply downregulated in GPCs derived from three patients (lines 8, 51, and 164) but not in a fourth (line 29), which was instead associated with sharp downregulation of LINGO1, DSCAML1, and several neurexins and neuroexophilins; these data suggest heterogeneity of transcriptional dysfunction that may lead to a final common pathway of glia-involved synaptic dysfunction in SCZ (Tables S2 and S3). These transcripts are critical contributors to synaptic stabilization and function (Südhof, 2008) but, although typically considered neuronal, may be produced significantly by glial cells as well (Zhang et al., 2014). The relative downregulation of these genes by SCZ hGPCs may reflect the suppression of mature glial transcripts in these cells, coincident with their relative block in glial differentiation. This, in turn, may lead to a relative failure of SCZ hGPCs and their derived astrocytes to provide these key proteins to their neuronal partners as well as a potential failure on the part of glial progenitors receiving synaptic inputs to respond to afferent stimulation (De Biase et al., 2010; Lin and Bergles, 2004). Thus, besides the structural havoc that might be expected of a cortical connectome formed without normal astrocytic support, the synaptic structure of the resultant networks might be expected to be destabilized by poor SCZ glial provision to the synaptic cleft of key astrocytic proteins required for normal synaptic maintenance and function.

SCZ is genetically heterogeneous, so anatomic and behavioral pathology may vary significantly among animals chimerized with GPCs derived from different patients. It is thus critical that the results obtained from chimeras established with control hiPSC GPCs be stable across both distinct lines of donor cells and among recipient mice. The chimeric brains established from the hGPCs of three different SCZ patients were thus compared anatomically with those established from GPCs derived from three control patients. None of the controls manifested the white matter-avoidant dispersal pattern of the SCZ hGPC chimeras. Similarly, we never noted this pattern of SCZ hGPC avoidance of the white matter in any of several hundred human glial chimeras engrafted in other studies with either fetal tissue-derived (Windrem et al., 2008, 2014) or normal iPSC-derived (Wang et al., 2013) hGPCs.

Besides their clear anatomic phenotype, SCZ hGPC-chimeric mice manifested robust behavioral phenotypes. They exhibited significantly attenuated prepulse inhibition relative to control-engrafted mice, relative anhedonia, excessive anxiety, deficient socialization with avoidance of conspecifics, and disrupted patterns of diurnal activity and sleep. These data establish that SCZ glial engraftment may yield an abnormal behavioral phenotype in recipient mice along behavioral axes that typify selected aspects of schizophrenic behavioral pathology in humans. In that regard, although extensive literature has implicated GPCs (Bergles et al., 2010; De Biase et al., 2010) as well as astroglia (Araque et al., 1998; Kang et al., 1998) in the modulation of synaptic plasticity and learning (Han et al., 2013), our data do not implicate one phenotype over the other in the modulation of behavior by SCZ glial chimerization; our chimeric mice are colonized by both donor-derived human GPCs and their derived astrocytes. That said, our observations of significant defects in SCZ glial maturation shared by hGPCs derived from multiple independent patients, associated in each with hypomyelination and disrupted astrocytic differentiation as well as with abnormal behavioral phenotypes in

(F and G) The diurnal activity and sleep patterns of adult mice (70–80 weeks old) engrafted neonatally with either SCZ or CTRL hGPCs were assessed for 72 hr in closed chambers (Noldus Ethovision) under continuous video recording.

(F) The average distance traveled in meters/hour over a 72-hr period was calculated and compared between CTRL mice (gray fill, n = 8 mice; lines 22 and 17) and SCZ mice (purple fill; n = 10, line 52). Time of day is shown as a 24-hr cycle, with the dark phase indicated by gray background shading. SCZ mice were significantly more active throughout the observation period than CTRL-engrafted mice ($p < 0.0001$, ANOVA, $F = 19.32$ [1,851].

(G) Left: Sample heatmaps of 1 hr of activity during the light phase (16:00, second day in box), the normal period of sleep for mice. The control mouse (left) remains inactive for the entire hour, whereas the SCZ mouse moves about the cage during much of the hour. Right: SCZ mice exhibited sleep patterns that were fragmented into bouts of shorter duration than their normal hGPC chimeric controls ($p = 0.0026$ by ANOVA, $F = 12.08$ [1,24]). Means ± SEM; unpaired, two-tailed Welch-corrected t tests.

the resultant SCZ GPC chimeras, together suggest a strong causal contribution of glial pathology to SCZ. In addition, these data highlight the potential of disease-specific humanized chimeras in defining the respective contributions of glial and neuronal dysfunction in the genesis and course of neurological disease.

STAR★METHODS

Detailed methods are provided in the online version of this paper and include the following:

- KEY RESOURCES TABLE
- CONTACT FOR REAGENT AND RESOURCE SHARING
- EXPERIMENTAL MODEL AND SUBJECT DETAILS
  - Patient identification, protection and sampling
  - iPSC line derivation and production of GPCs
  - Host transplantation
- METHOD DETAILS
  - Transplantation
  - Immunolabeling of tissue sections
  - Western blots
  - Behavior
  - Activity and sleep assessment
  - RNA-seq
- QUANTIFICATION AND STATISTICAL ANALYSIS
  - Imaging and quantitative histology
  - Astrocyte morphometrics
  - Myelin luminance analysis
  - Statistical analysis
  - Bioinformatics
  - Real-Time PCR
- DATA AND SOFTWARE AVAILABILITY

SUPPLEMENTAL INFORMATION

Supplemental Information includes five figures and three tables and can be found with this article online at http://dx.doi.org/10.1016/j.stem.2017.06.012.

AUTHOR CONTRIBUTIONS

M.O. performed the genomic analysis. D.C.M. and Z.L. prepared RNA and validated both RNA and protein expression. J.B., D.C.M., and Z.L. raised cells under the direction of S.W. J.M., S.S., and L.Z. assessed myelination and astrocytic morphologies under the direction of M.S.W. R.H.M. and P.J.T. produced the iPSCs from patient samples provided by R.L.F. L.Z. and K.M. performed the blinded behavioral analyses, and M.N. and M.S.W. analyzed the behavioral and sleep data. M.S.W. organized the histological and behavioral figures, and M.O. organized the genomics figures and tables. P.J.T., M.S.W., M.N., and S.A.G. conceived the project. S.A.G. directed the overall effort and wrote the paper.

ACKNOWLEDGMENTS

This work was supported by NIMH grants R01MH099578 and R01MH104701, NINDS R01NS75345, the G. Harold and Leila Y. Mathers Charitable Foundation, the Dr. Miriam and Sheldon G. Adelson Medical Research Foundation, and the Novo Nordisk Foundation. We thank Alexis Yagielski and Simrat Dhaliwal for histological assistance, Jennifer Wintermute for assistance with cell culture, Lorenz Studer (Memorial Sloan Kettering) for the C27 hiPSC cell line, Nora McNamara (Case Western) for assistance with patient identification, Leslie Cooperman and Elizabeth Shick (Case Western) for assistance with producing the iPSC lines, and Chiara Cirelli (University of Wisconsin) for her comments on our sleep and activity data. This paper is dedicated to the memory of Mr. James T. Handelman of the Mathers Charitable Foundation, whose early and ardent support made this work possible. Drs. Goldman and Windrem hold a patent on human glial chimeric mice, US 7,524,491, from which they receive no financial remuneration.

Received: March 21, 2017
Revised: May 2, 2017
Accepted: June 19, 2017
Published: July 20, 2017

REFERENCES

Aberg, K., Saetre, P., Jareborg, N., and Jazin, E. (2006). Human QKI, a potential regulator of mRNA expression of human oligodendrocyte-related genes involved in schizophrenia. Proc. Natl. Acad. Sci. USA *103*, 7482–7487.

Amaral, A.I., Meisingset, T.W., Kotter, M.R., and Sonnewald, U. (2013). Metabolic aspects of neuron-oligodendrocyte-astrocyte interactions. Front. Endocrinol. (Lausanne) *4*, 54.

Andrews, J.L., and Fernandez-Enright, F. (2015). A decade from discovery to therapy: Lingo-1, the dark horse in neurological and psychiatric disorders. Neurosci. Biobehav. Rev. *56*, 97–114.

Araque, A., Parpura, V., Sanzgiri, R.P., and Haydon, P.G. (1998). Glutamate-dependent astrocyte modulation of synaptic transmission between cultured hippocampal neurons. Eur. J. Neurosci. *10*, 2129–2142.

Barnes, S.A., Der-Avakian, A., and Markou, A. (2014). Anhedonia, avolition, and anticipatory deficits: assessments in animals with relevance to the negative symptoms of schizophrenia. Eur. Neuropsychopharmacol. *24*, 744–758.

Barres, B.A., and Raff, M.C. (1993). Proliferation of oligodendrocyte precursor cells depends on electrical activity in axons. Nature *361*, 258–260.

Bergles, D.E., Jabs, R., and Steinhäuser, C. (2010). Neuron-glia synapses in the brain. Brain Res. Brain Res. Rev. *63*, 130–137.

Bevins, R.A., and Besheer, J. (2006). Object recognition in rats and mice: a one-trial non-matching-to-sample learning task to study 'recognition memory'. Nat. Protoc. *1*, 1306–1311.

Bolger, A.M., Lohse, M., and Usadel, B. (2014). Trimmomatic: a flexible trimmer for Illumina sequence data. Bioinformatics *30*, 2114–2120.

Chambers, S.M., Fasano, C.A., Papapetrou, E.P., Tomishima, M., Sadelain, M., and Studer, L. (2009). Highly efficient neural conversion of human ES and iPS cells by dual inhibition of SMAD signaling. Nat. Biotechnol. *27*, 275–280.

Clarke, L.E., and Barres, B.A. (2013). Glia keep synapse distribution under wraps. Cell *154*, 267–268.

Connor, C.M., Crawford, B.C., and Akbarian, S. (2011). White matter neuron alterations in schizophrenia and related disorders. Int. J. Dev. Neurosci. *29*, 325–334.

D'Antonio, M., D'Onorio De Meo, P., Pallocca, M., Picardi, E., D'Erchia, A.M., Calogero, R.A., Castrignanò, T., and Pesole, G. (2015). RAP: RNA-Seq Analysis Pipeline, a new cloud-based NGS web application. BMC Genomics *16*, S3.

Dang, V., Medina, B., Das, D., Moghadam, S., Martin, K.J., Lin, B., Naik, P., Patel, D., Nosheny, R., Wesson Ashford, J., and Salehi, A. (2014). Formoterol, a long-acting β2 adrenergic agonist, improves cognitive function and promotes dendritic complexity in a mouse model of Down syndrome. Biol. Psychiatry *75*, 179–188.

Davis, K.L., Stewart, D.G., Friedman, J.I., Buchsbaum, M., Harvey, P.D., Hof, P.R., Buxbaum, J., and Haroutunian, V. (2003). White matter changes in schizophrenia: evidence for myelin-related dysfunction. Arch. Gen. Psychiatry *60*, 443–456.

De Biase, L.M., Nishiyama, A., and Bergles, D.E. (2010). Excitability and synaptic communication within the oligodendrocyte lineage. J. Neurosci. *30*, 3600–3611.

Ewing, S.G., and Grace, A.A. (2013). Evidence for impaired sound intensity processing during prepulse inhibition of the startle response in a rodent developmental disruption model of schizophrenia. J. Psychiatr. Res. *47*, 1630–1635.

Fagerland, M.W., and Sandvik, L. (2009). Performance of five two-sample location tests for skewed distributions with unequal variances. Contemp. Clin. Trials *30*, 490–496.

Fernandez-Enright, F., Andrews, J.L., Newell, K.A., Pantelis, C., and Huang, X.F. (2014). Novel implications of Lingo-1 and its signaling partners in schizophrenia. Transl. Psychiatry *4*, e348.

Fields, R.D. (2008). White matter in learning, cognition and psychiatric disorders. Trends Neurosci. *31*, 361–370.

Franklin, R.J., and Bussey, T.J. (2013). Do your glial cells make you clever? Cell Stem Cell *12*, 265–266.

Gentleman, R.C., Carey, V.J., Bates, D.M., Bolstad, B., Dettling, M., Dudoit, S., Ellis, B., Gautier, L., Ge, Y., Gentry, J., et al. (2004). Bioconductor: open software development for computational biology and bioinformatics. Genome Biol. *5*, R80.

Georgieva, L., Moskvina, V., Peirce, T., Norton, N., Bray, N.J., Jones, L., Holmans, P., Macgregor, S., Zammit, S., Wilkinson, J., et al. (2006). Convergent evidence that oligodendrocyte lineage transcription factor 2 (OLIG2) and interacting genes influence susceptibility to schizophrenia. Proc. Natl. Acad. Sci. USA *103*, 12469–12474.

Geyer, M.A., and Swerdlow, N.R. (2001). Measurement of startle response, prepulse inhibition, and habituation. Curr. Protoc. Neurosci. *Chapter 8*. Unit 8.7.

Gogtay, N., and Rapoport, J.L. (2008). Childhood-onset schizophrenia: insights from neuroimaging studies. J. Am. Acad. Child Adolesc. Psychiatry *47*, 1120–1124.

Gogtay, N., Lu, A., Leow, A.D., Klunder, A.D., Lee, A.D., Chavez, A., Greenstein, D., Giedd, J.N., Toga, A.W., Rapoport, J.L., and Thompson, P.M. (2008). Three-dimensional brain growth abnormalities in childhood-onset schizophrenia visualized by using tensor-based morphometry. Proc. Natl. Acad. Sci. USA *105*, 15979–15984.

Goldman, S.A., Nedergaard, M., and Windrem, M.S. (2015). Modeling cognition and disease using human glial chimeric mice. Glia *63*, 1483–1493.

Graw, S.L., Swisshelm, K., Floyd, K., Carstens, B.J., Wamboldt, M.Z., Ross, R.G., and Leonard, S. (2012). Isochromosome 13 in a patient with childhood-onset schizophrenia, ADHD, and motor tic disorder. Mol. Cytogenet. *5*, 2.

Hakak, Y., Walker, J.R., Li, C., Wong, W.H., Davis, K.L., Buxbaum, J.D., Haroutunian, V., and Fienberg, A.A. (2001). Genome-wide expression analysis reveals dysregulation of myelination-related genes in chronic schizophrenia. Proc. Natl. Acad. Sci. USA *98*, 4746–4751.

Han, X., Chen, M., Wang, F., Windrem, M., Wang, S., Shanz, S., Xu, Q., Oberheim, N.A., Bekar, L., Betstadt, S., et al. (2013). Forebrain engraftment by human glial progenitor cells enhances synaptic plasticity and learning in adult mice. Cell Stem Cell *12*, 342–353.

Hof, P.R., Haroutunian, V., Copland, C., Davis, K.L., and Buxbaum, J.D. (2002). Molecular and cellular evidence for an oligodendrocyte abnormality in schizophrenia. Neurochem. Res. *27*, 1193–1200.

Horrobin, D.F. (1998). Schizophrenia: the illness that made us human. Med. Hypotheses *50*, 269–288.

Ivleva, E.I., Moates, A.F., Hamm, J.P., Bernstein, I.H., O'Neill, H.B., Cole, D., Clementz, B.A., Thaker, G.K., and Tamminga, C.A. (2014). Smooth pursuit eye movement, prepulse inhibition, and auditory paired stimuli processing endophenotypes across the schizophrenia-bipolar disorder dimension. Schizophr. Bull. *40*, 642–652.

Jacomy, M., Venturini, T., Heymann, S., and Bastian, M. (2014). ForceAtlas2, a continuous graph layout algorithm for handy network visualization designed for the Gephi software. PLoS ONE *9*, e98679.

John, G.R. (2012). Investigation of astrocyte - oligodendrocyte interactions in human cultures. Methods Mol. Biol. *814*, 401–414.

Kaimal, V., Bardes, E.E., Tabar, S.C., Jegga, A.G., and Aronow, B.J. (2010). ToppCluster: a multiple gene list feature analyzer for comparative enrichment clustering and network-based dissection of biological systems. Nucleic Acids Res. *38*, W96–W102.

Kang, J., Jiang, L., Goldman, S.A., and Nedergaard, M. (1998). Astrocyte-mediated potentiation of inhibitory synaptic transmission. Nat. Neurosci. *1*, 683–692.

Kohl, S., Heekeren, K., Klosterkötter, J., and Kuhn, J. (2013). Prepulse inhibition in psychiatric disorders–apart from schizophrenia. J. Psychiatr. Res. *47*, 445–452.

Langmead, B., and Salzberg, S.L. (2012). Fast gapped-read alignment with Bowtie 2. Nat. Methods *9*, 357–359.

Lee, Y., Morrison, B.M., Li, Y., Lengacher, S., Farah, M.H., Hoffman, P.N., Liu, Y., Tsingalia, A., Jin, L., Zhang, P.W., et al. (2012). Oligodendroglia metabolically support axons and contribute to neurodegeneration. Nature *487*, 443–448.

Li, P., Piao, Y., Shon, H.S., and Ryu, K.H. (2015). Comparing the normalization methods for the differential analysis of Illumina high-throughput RNA-Seq data. BMC Bioinformatics *16*, 347.

Liao, Y., Smyth, G.K., and Shi, W. (2013). The Subread aligner: fast, accurate and scalable read mapping by seed-and-vote. Nucleic Acids Res. *41*, e108.

Liao, Y., Smyth, G.K., and Shi, W. (2014). featureCounts: an efficient general purpose program for assigning sequence reads to genomic features. Bioinformatics *30*, 923–930.

Lin, S.C., and Bergles, D.E. (2004). Synaptic signaling between GABAergic interneurons and oligodendrocyte precursor cells in the hippocampus. Nat. Neurosci. *7*, 24–32.

Love, M.I., Huber, W., and Anders, S. (2014). Moderated estimation of fold change and dispersion for RNA-seq data with DESeq2. Genome Biol. *15*, 550.

Maćkowiak, M., Mordalska, P., and Wędzony, K. (2014). Neuroligins, synapse balance and neuropsychiatric disorders. Pharmacol. Rep. *66*, 830–835.

McIntosh, A.M., Muñoz Maniega, S., Lymer, G.K., McKirdy, J., Hall, J., Sussmann, J.E., Bastin, M.E., Clayden, J.D., Johnstone, E.C., and Lawrie, S.M. (2008). White matter tractography in bipolar disorder and schizophrenia. Biol. Psychiatry *64*, 1088–1092.

McShane, B.B., Galante, R.J., Jensen, S.T., Naidoo, N., Pack, A.I., and Wyner, A. (2010). Characterization of the bout durations of sleep and wakefulness. J. Neurosci. Methods *193*, 321–333.

Miller, J.A., Horvath, S., and Geschwind, D.H. (2010). Divergence of human and mouse brain transcriptome highlights Alzheimer disease pathways. Proc. Natl. Acad. Sci. USA *107*, 12698–12703.

Muñoz Maniega, S., Lymer, G.K., Bastin, M.E., Marjoram, D., Job, D.E., Moorhead, T.W., Owens, D.G., Johnstone, E.C., McIntosh, A.M., and Lawrie, S.M. (2008). A diffusion tensor MRI study of white matter integrity in subjects at high genetic risk of schizophrenia. Schizophr. Res. *106*, 132–139.

Najjar, S., and Pearlman, D.M. (2015). Neuroinflammation and white matter pathology in schizophrenia: systematic review. Schizophr. Res. *161*, 102–112.

Oberheim, N.A., Wang, X., Goldman, S., and Nedergaard, M. (2006). Astrocytic complexity distinguishes the human brain. Trends Neurosci. *29*, 547–553.

Oberheim, N.A., Takano, T., Han, X., He, W., Lin, J.H., Wang, F., Xu, Q., Wyatt, J.D., Pilcher, W., Ojemann, J.G., et al. (2009). Uniquely hominid features of adult human astrocytes. J. Neurosci. *29*, 3276–3287.

Pack, A.I., Galante, R.J., Maislin, G., Cater, J., Metaxas, D., Lu, S., Zhang, L., Von Smith, R., Kay, T., Lian, J., et al. (2007). Novel method for high-throughput phenotyping of sleep in mice. Physiol. Genomics *28*, 232–238.

Pruitt, K.D., Tatusova, T., and Maglott, D.R. (2007). NCBI reference sequences (RefSeq): a curated non-redundant sequence database of genomes, transcripts and proteins. Nucleic Acids Res. *35*, D61–D65.

Rapoport, J.L., Addington, A.M., Frangou, S., and Psych, M.R. (2005). The neurodevelopmental model of schizophrenia: update 2005. Mol. Psychiatry *10*, 434–449.

R Core Team (2016). R: A language and environment for statistical computing. R Foundation for Statistical Computing, Vienna, Austria. https://www.R-project.org/.

Risso, D., Schwartz, K., Sherlock, G., and Dudoit, S. (2011). GC-Content Normalization for RNA-Seq Data. BMC Bioinformatics *12*, 480.

Risso, D., Ngai, J., Speed, T.P., and Dudoit, S. (2014). Normalization of RNA-seq data using factor analysis of control genes or samples. Nat. Biotechnol. *32*, 896–902.

Roach, A., Boylan, K., Horvath, S., Prusiner, S.B., and Hood, L.E. (1983). Characterization of cloned cDNA representing rat myelin basic protein: absence of expression in brain of shiverer mutant mice. Cell *34*, 799–806.

Robinson, M.D., McCarthy, D.J., and Smyth, G.K. (2010). edgeR: a Bioconductor package for differential expression analysis of digital gene expression data. Bioinformatics *26*, 139–140.

Rosenbluth, J. (1980). Central myelin in the mouse mutant shiverer. J. Comp. Neurol. *194*, 639–648.

Roy, K., Murtie, J.C., El-Khodor, B.F., Edgar, N., Sardi, S.P., Hooks, B.M., Benoit-Marand, M., Chen, C., Moore, H., O'Donnell, P., et al. (2007). Loss of erbB signaling in oligodendrocytes alters myelin and dopaminergic function, a potential mechanism for neuropsychiatric disorders. Proc. Natl. Acad. Sci. USA *104*, 8131–8136.

Sakry, D., Neitz, A., Singh, J., Frischknecht, R., Marongiu, D., Binamé, F., Perera, S.S., Endres, K., Lutz, B., Radyushkin, K., et al. (2014). Oligodendrocyte precursor cells modulate the neuronal network by activity-dependent ectodomain cleavage of glial NG2. PLoS Biol. *12*, e1001993.

Salyakina, D., Cukier, H.N., Lee, J.M., Sacharow, S., Nations, L.D., Ma, D., Jaworski, J.M., Konidari, I., Whitehead, P.L., Wright, H.H., et al. (2011). Copy number variants in extended autism spectrum disorder families reveal candidates potentially involved in autism risk. PLoS ONE *6*, e26049.

Samartzis, L., Dima, D., Fusar-Poli, P., and Kyriakopoulos, M. (2014). White matter alterations in early stages of schizophrenia: a systematic review of diffusion tensor imaging studies. J. Neuroimaging *24*, 101–110.

Shinkai, Y., Rathbun, G., Lam, K.P., Oltz, E.M., Stewart, V., Mendelsohn, M., Charron, J., Datta, M., Young, F., Stall, A.M., et al. (1992). RAG-2-deficient mice lack mature lymphocytes owing to inability to initiate V(D)J rearrangement. Cell *68*, 855–867.

Sholl, D.A. (1953). Dendritic organization in the neurons of the visual and motor cortices of the cat. J. Anat. *87*, 387–406.

Sigmundsson, T., Suckling, J., Maier, M., Williams, S., Bullmore, E., Greenwood, K., Fukuda, R., Ron, M., and Toone, B. (2001). Structural abnormalities in frontal, temporal, and limbic regions and interconnecting white matter tracts in schizophrenic patients with prominent negative symptoms. Am. J. Psychiatry *158*, 234–243.

Sim, F.J., Windrem, M.S., and Goldman, S.A. (2009). Fate determination of adult human glial progenitor cells. Neuron Glia Biol. *5*, 45–55.

Sim, F.J., McClain, C.R., Schanz, S.J., Protack, T.L., Windrem, M.S., and Goldman, S.A. (2011). CD140a identifies a population of highly myelinogenic, migration-competent and efficiently engrafting human oligodendrocyte progenitor cells. Nat. Biotechnol. *29*, 934–941.

Simons, M., and Nave, K.A. (2015). Oligodendrocytes: Myelination and Axonal Support. Cold Spring Harb. Perspect. Biol. *8*, a020479.

Somers, A., Jean, J.C., Sommer, C.A., Omari, A., Ford, C.C., Mills, J.A., Ying, L., Sommer, A.G., Jean, J.M., Smith, B.W., et al. (2010). Generation of transgene-free lung disease-specific human induced pluripotent stem cells using a single excisable lentiviral stem cell cassette. Stem Cells *28*, 1728–1740.

Südhof, T.C. (2008). Neuroligins and neurexins link synaptic function to cognitive disease. Nature *455*, 903–911.

Takahashi, K., Tanabe, K., Ohnuki, M., Narita, M., Ichisaka, T., Tomoda, K., and Yamanaka, S. (2007). Induction of pluripotent stem cells from adult human fibroblasts by defined factors. Cell *131*, 861–872.

Takahashi, N., Sakurai, T., Davis, K.L., and Buxbaum, J.D. (2011). Linking oligodendrocyte and myelin dysfunction to neurocircuitry abnormalities in schizophrenia. Prog. Neurobiol. *93*, 13–24.

Ullian, E.M., Sapperstein, S.K., Christopherson, K.S., and Barres, B.A. (2001). Control of synapse number by glia. Science *291*, 657–661.

Uranova, N.A., Vostrikov, V.M., Vikhreva, O.V., Zimina, I.S., Kolomeets, N.S., and Orlovskaya, D.D. (2007). The role of oligodendrocyte pathology in schizophrenia. Int. J. Neuropsychopharmacol. *10*, 537–545.

Uranova, N.A., Vikhreva, O.V., Rachmanova, V.I., and Orlovskaya, D.D. (2011). Ultrastructural alterations of myelinated fibers and oligodendrocytes in the prefrontal cortex in schizophrenia: a postmortem morphometric study. Schizophr. Res. Treatment *2011*, 325789.

Voineskos, A.N., Felsky, D., Kovacevic, N., Tiwari, A.K., Zai, C., Chakravarty, M.M., Lobaugh, N.J., Shenton, M.E., Rajji, T.K., Miranda, D., et al. (2013). Oligodendrocyte genes, white matter tract integrity, and cognition in schizophrenia. Cereb. Cortex *23*, 2044–2057.

Walf, A.A., and Frye, C.A. (2007). The use of the elevated plus maze as an assay of anxiety-related behavior in rodents. Nat. Protoc. *2*, 322–328.

Walsh, T., McClellan, J.M., McCarthy, S.E., Addington, A.M., Pierce, S.B., Cooper, G.M., Nord, A.S., Kusenda, M., Malhotra, D., Bhandari, A., et al. (2008). Rare structural variants disrupt multiple genes in neurodevelopmental pathways in schizophrenia. Science *320*, 539–543.

Wang, S., Bates, J., Li, X., Schanz, S., Chandler-Militello, D., Levine, C., Maherali, N., Studer, L., Hochedlinger, K., Windrem, M., and Goldman, S.A. (2013). Human iPSC-derived oligodendrocyte progenitor cells can myelinate and rescue a mouse model of congenital hypomyelination. Cell Stem Cell *12*, 252–264.

Welstead, G.G., Brambrink, T., and Jaenisch, R. (2008). Generating iPS cells from MEFS through forced expression of Sox-2, Oct-4, c-Myc, and Klf4. J. Vis. Exp. *14*, 734.

Willner, P., Towell, A., Sampson, D., Sophokleous, S., and Muscat, R. (1987). Reduction of sucrose preference by chronic unpredictable mild stress, and its restoration by a tricyclic antidepressant. Psychopharmacology (Berl.) *93*, 358–364.

Windrem, M.S., Nunes, M.C., Rashbaum, W.K., Schwartz, T.H., Goodman, R.A., McKhann, G., 2nd, Roy, N.S., and Goldman, S.A. (2004). Fetal and adult human oligodendrocyte progenitor cell isolates myelinate the congenitally dysmyelinated brain. Nat. Med. *10*, 93–97.

Windrem, M.S., Schanz, S.J., Guo, M., Tian, G.F., Washco, V., Stanwood, N., Rasband, M., Roy, N.S., Nedergaard, M., Havton, L.A., et al. (2008). Neonatal chimerization with human glial progenitor cells can both remyelinate and rescue the otherwise lethally hypomyelinated shiverer mouse. Cell Stem Cell *2*, 553–565.

Windrem, M.S., Schanz, S.J., Morrow, C., Munir, J., Chandler-Militello, D., Wang, S., and Goldman, S.A. (2014). A competitive advantage by neonatally engrafted human glial progenitors yields mice whose brains are chimeric for human glia. J. Neurosci. *34*, 16153–16161.

Xia, M., Abazyan, S., Jouroukhin, Y., and Pletnikov, M. (2016). Behavioral sequelae of astrocyte dysfunction: focus on animal models of schizophrenia. Schizophr. Res. *176*, 72–82.

Yang, M., Silverman, J.L., and Crawley, J.N. (2011). Automated three-chambered social approach task for mice. Curr. Protoc. Neurosci. *Chapter 8*. Unit 826.

Zhang, Y., Chen, K., Sloan, S.A., Bennett, M.L., Scholze, A.R., O'Keeffe, S., Phatnani, H.P., Guarnieri, P., Caneda, C., Ruderisch, N., et al. (2014). An RNA-sequencing transcriptome and splicing database of glia, neurons, and vascular cells of the cerebral cortex. J. Neurosci. *34*, 11929–11947.

Zhang, Y., Sloan, S.A., Clarke, L.E., Caneda, C., Plaza, C.A., Blumenthal, P.D., Vogel, H., Steinberg, G.K., Edwards, M.S., Li, G., et al. (2016). Purification and characterization of progenitor and mature human astrocytes reveals transcriptional and functional differences with mouse. Neuron *89*, 37–53.

Zimmerman, D.W. (2004). A note on preliminary tests of equality of variances. Br. J. Math. Stat. Psychol. *57*, 173–181.

Zou, X.Y., Yang, H.Y., Yu, Z., Tan, X.B., Yan, X., and Huang, G.T. (2012). Establishment of transgene-free induced pluripotent stem cells reprogrammed from human stem cells of apical papilla for neural differentiation. Stem Cell Res. Ther. *3*, 43.

STAR★METHODS

KEY RESOURCES TABLE

REAGENT or RESOURCE	SOURCE	IDENTIFIER
Antibodies		
Rat monoclonal anti-myelin basic protein, 1:25	Abcam	Cat#ab7349; RRID: AB_305869
Rabbit polyclonal anti-transferrin, 1:800	Abcam	Cat#ab9538; RRID: AB_307325
Mouse monoclonal anti-human GFAP, clone SMI 21R, 1:500	Covance Research Products	Cat#SMI-21R-500; RRID: AB_509979
Rabbit monoclonal anti-Ki-67, clone SP6	ThermoFisher Scientific	Cat#RM-9106-S
Mouse monoclonal anti-human cytoplasmic marker	Takara Bio	Cat#aB-121-U-050; RRID: AB_2632385
Rat monoclonal anti-BrdU clone BU1/75 (ICR1)	Bio-Rad	Cat#MCA2060; RRID: AB_323427
Rabbit polyclonal anti-Olig2, 1:500	Neuromics	Cat#RA25017, 25081
Mouse anti-NG2, clone 9.2.27, 1:200	Millipore	Cat#MAB2029
Rabbit monoclonal anti-PDGF Receptor alpha, clone D13C6, 1:300	Cell Signaling Technology	Cat#5241S; RRID: AB_10692773
Goat anti-mouse IgG (H+L) Alexa Fluor 647, 1:400	ThermoFisher Scientific	Cat#A-21235; RRID: AB_2535804
Goat anti-mouse IgG1 Alexa Fluor 488, 1:400	ThermoFisher Scientific	Cat#A-21121; RRID: AB_2535764
Goat anti-mouse IgG (H+L) Alexa Fluor 488, 1:400	ThermoFisher Scientific	Cat#A-11029; RRID: AB_2534088
Goat anti-mouse IgG (H+L) Alexa Fluor 568, 1:400	ThermoFisher Scientific	Cat#A-11031; RRID: AB_144696
Goat anti-mouse IgG1 Alexa Fluor 568, 1:400	ThermoFisher Scientific	Cat#A-21124; RRID: AB_2535766
Goat anti-rabbit IgG (H+L) Alexa Fluor 647, 1:400	ThermoFisher Scientific	Cat#A-21245; RRID: AB_2535813
Goat anti-rabbit IgG (H+L) Alexa Fluor 568, 1:400	ThermoFisher Scientific	Cat#A-11036; RRID: AB_2534094
Goat anti-rabbit IgG (H+L) Alexa Fluor 488, 1:400	ThermoFisher Scientific	Cat#A-11034; RRID: AB_2576217
Goat anti-rat IgG (H+L) Alexa Fluor 647, 1:400	ThermoFisher Scientific	Cat#A-21247; RRID: AB_141778
Goat anti-rat IgG (H+L) Alexa Fluor 568, 1:400	ThermoFisher Scientific	Cat#A-11077; RRID: AB_2534121
Goat anti-rat IgG (H+L) Alexa Fluor 488, 1:400	ThermoFisher Scientific	Cat#A-11006; RRID: AB_2534074
Alexa Fluor 488-SSEA4	Invitrogen	Cat#A14810
APC-conjugated mouse IgG1, Isotype Control, 1:10	Miltenyi Biotec	Cat#130-092-214
APC-mouse IgM, Isotype Control, 1:40	Miltenyi Biotec	Cat#130-093-176
APC-conjugated mAb A2B5, 1:40	Miltenyi Biotec	Cat#130-093-582
APC-conjugated anti-CD44, 1:500	Miltenyi Biotec	Cat#130-095-177
APC-conjugated anti-CD133/1, 1:10	Miltenyi Biotec	Cat#130-090-826
PE-conjugated anti-CD140a, 1:10	BD Pharmingen	Cat#556002
anti-Olig2, 1:200	R&D Systems	Cat#AF2418
PE-conj. anti-mouse IgG2a, isotype control, 1:10	BD Pharmingen	Cat#555574
anti-PDGF alpha receptor, 1:200	Cell Signaling Tech.	Cat#5241S
anti-Neurexin 1, 1:1000	EMD Millipore	ABN161-1
Chemicals, Peptides, and Recombinant Proteins		
bFGF	Sigma	Cat#F0291
Biotin	Sigma	Cat#B4639
dibutyryl cAMP	Sigma	Cat#D0260
Heparin	Fisher	Cat#NC9484621
IGF-1	R&D Systems	Cat#291-G1-050
Laminin	Corning	Cat#354232
NT3	R&D Systems	Cat#267-N3-025
PDGFaa	R&D Systems	Cat#221-AA-50

(*Continued on next page*)

Continued

REAGENT or RESOURCE	SOURCE	IDENTIFIER
Purmorphamine	Calbiochem	Cat#80603-730
Retinoic acid	Sigma	Cat#R2625
T3	Sigma	Cat#T5516-1MG
Critical Commercial Assays		
Custom TaqMan Array Card	Applied Biosystems	N/A
Ovation PicoSL WTA System V2	NuGEN	Cat#3312
RNeasy mini kit	QIAGEN	Cat#74104
Taqman Universal master mix	Applied Biosystems	Cat #4304437
TruSeq RNA library Prep Kit V2	Illumina	Cat#RS-122-2001
Deposited Data		
Raw RNA-seq data	GEO datasets: https://www.ncbi.nlm.nih.gov/gds/	GEO: GSE86906
Processed RNA-seq data (count matrix) and R scripts for data analysis	This paper	GitHub: https://github.com/cbtncph/GoldmanetalSCZ2016
Human reference genome NCBI build 38, GRCh38	Genome Reference Consortium	https://www.ncbi.nlm.nih.gov/grc/human
Experimental Models: Cell Lines		
C27	L. Studer, Sloan-Kettering Institute	N/A
CWRU8	P. Tesar, Case Western	N/A
CWRU19	P. Tesar, Case Western	N/A
CWRU22	P. Tesar, Case Western	N/A
CWRU29	P. Tesar, Case Western	N/A
CWRU31	P. Tesar, Case Western	N/A
CWRU37	P. Tesar, Case Western	N/A
CWRU51	P. Tesar, Case Western	N/A
CWRU52	P. Tesar, Case Western	N/A
CWRU164	P. Tesar, Case Western	N/A
CWRU193	P. Tesar, Case Western	N/A
CWRU205	P. Tesar, Case Western	N/A
Experimental Models: Organisms/Strains		
Mouse: C3Fe.SWV-Mbpshi/J	Jackson Laboratory	Cat#001428
Mouse: B6.129S7-Rag1tm1Mom/J	Jackson Laboratory	Cat#002216
Mouse: C3H.129S6(B6)-Rag2tm1FwaN12	Taconic	Cat#000602-M
Software and Algorithms		
Photoshop CS6	Adobe	N/A
Illustrator CS6	Adobe	N/A
StereoInvestigator v11	MBF Bioscience	N/A
Neurolucida 360 v2	MBF Bioscience	N/A
Neurolucida Explorer v11	MBF Bioscience	N/A
Leica Metamorph AF v2	Leica Biosystems	N/A
Leica Application Suite X	Leica Biosystems	N/A
FlowJo	TreeStar	N/A
Trimmomatic (version 0.32)	Bolger et al. (2014)	http://www.usadellab.org/cms/?page=trimmomatic
Subread (version 1.4.6-p3)	Liao et al. (2013)	http://subread.sourceforge.net/
featureCounts (version 1.4.6-p3)	Liao et al. (2014)	http://subread.sourceforge.net/
R	R Core Team (2016)	https://www.R-project.org/
RUVSeq (version 1.6.2)	Risso et al. (2014)	http://www.bioconductor.org/packages/release/bioc/html/RUVSeq.html

(*Continued on next page*)

Continued

REAGENT or RESOURCE	SOURCE	IDENTIFIER
EDASeq (version 2.6.2)	Risso et al. (2011)	http://www.bioconductor.org/packages/release/bioc/html/EDASeq.html
edgeR (version 3.14.0)	Robinson et al. (2010)	http://www.bioconductor.org/packages/release/bioc/html/edgeR.html
DESeq2 (version 1.12.4)	Love et al. (2014)	http://www.bioconductor.org/packages/release/bioc/html/DESeq2.html
ToppCluster	Kaimal et al. (2010)	https://toppcluster.cchmc.org/
Gephi (version 0.9.1)	https://gephi.org/	https://gephi.org/
Ingenuity Pathway Analysis	QIAGEN	https://www.qiagenbioinformatics.com/products/ingenuity-pathway-analysis/
ExpressionSuite Software (v.1.1)	Applied Biosystems	https://www.thermofisher.com/dk/en/home/technical-resources/software-downloads/expressionsuite-software.html
Other		
Orca-R2 Digital CCD Camera	Hamamatsu	Cat#C10600-10B
MAC 5000	Ludl Electronic Prods.	Cat#73005001
Focus DR Linear encoder	Ludl Electronic Prods.	Cat#99A420
STG 4"x3" Stepper	Ludl Electronic Prods.	Cat#99S100LE2MBF
Agilent Bioanalyzer	Agilent	N/A
BD FACS Aria IIIU	BD Biosciences	N/A
HiSeq 2500	Illumina	N/A
Nanodrop 1000 spectrophotometer	Nanodrop	N/A
QuantStudio 12K Flex Real-Time PCR system	Applied Biosystems	N/A

CONTACT FOR REAGENT AND RESOURCE SHARING

Further information and requests for resources and reagents should be directed to, and will be fulfilled by, the lead and corresponding author, Steve Goldman (goldman@sund.ku.dk or steven_goldman@urmc.rochester.edu).

EXPERIMENTAL MODEL AND SUBJECT DETAILS

Patient identification, protection and sampling

Patients from which these lines were derived were diagnosed with disabling degrees of schizophrenia with onset in early adolescence; informed consent was obtained and all patients and their guardians consented by a child psychiatrist (RLF) under an approved protocol of Case Western School of Medicine, blinded as to subsequent line designations, and no study investigators had access to patient identifiers.

iPSC line derivation and production of GPCs

Punch biopsies of the skin were obtained from patients with juvenile onset schizophrenia (ages 10 to 17 years old) and controls (ages 24 to 32 years old). The ages, genders, and ethnicities of each line used in this study are individually identified in Table S1. In brief, 4 control subjects were used: CTRL 1 (lines 19, 22; 26 year-old male); CTRL 2 (line 37; 32 year-old female); CTRL 3 (line 205; 25 year-old male); CTRL 4 (line C27, fully de-identified), while 5 schizophrenic patients were used: SCZ 1 (line 8; 10 year-old female); SCZ 2 (lines 51, 52; 16 year-old male); SCZ 3 (lines 29, 31; 12 year-old male); SCZ 4 (line 164; 14 year old female); SCZ 5 (line 193, 15 year-old female).

Induced pluripotent stem cells (iPSC) lines were derived from these patient samples using an excisable floxed polycistronic hSTEMCCA lentiviral vector. Short tandem repeat (STR)-based DNA fingerprinting was used to confirm iPSC identity, as a match to original patient or control donor. Additional genotyping was performed using Illumina Omni5 SNP arrays; these data are available in dbGAP (http://www.ncbi.nlm.nih.gov/gap). The iPSCs were then driven toward a glial progenitor cell (GPC) fate using previously described protocols (Wang et al., 2013). Cells were harvested between 160-240 DIV, by which time most typically expressed the bipotential GPC marker PDGFαR/CD140a, while the remainder were A2B5^{+}/CD140a^{-} astrocytes. The karyotypes of all iPSC lines were assessed during glial differentiation to ensure genotypic stability of the cells utilized in all experiments presented here (karyotyping by WiCell, Madison, WI). All iPSCs showed a normal karyotype, except for line 51, which was found to have a balanced Robertsonian translocation of chromosome 13, an anomaly previously associated with juvenile-onset schizophrenia (Graw et al., 2012).

Host transplantation

Homozygous shiverer mice (The Jackson Laboratory, Bar Harbor, ME) were crossed with homozygous rag2 null immunodeficient mice (Shinkai et al., 1992) on the C3h background (Taconic, Germantown, NY, USA) to generate *shi/shi* x rag2$^{-/-}$ myelin-deficient, immunodeficient mice (Windrem et al., 2008). In addition, rag1$^{-/-}$ normally-myelinated immunodeficient mice (B6.129S7-*Rag1*^{tm1Mom}/J), were obtained from the Jackson Laboratory and bred in our lab. Suspensions of single-cells or small clusters of hiPSC-derived GPCs were spun down to 100,000 cells/μl. Neonates were anesthetized by cooling, and transplanted bilaterally in the corpus callosum with a total of 200,000 cells, as described (Windrem et al., 2004); see Method Details section for transplant procedure. At 4.5 months of age (*shi/shi* x rag2$^{-/-}$) or after completion of behavioral testing at 6-9 months (rag1$^{-/-}$ only), transplanted mice were anesthetized with pentobarbital, then perfusion fixed with cold HBSS$^{+/+}$ followed by 4% paraformaldehyde (PF) with a 2 hr post-fixation in cold PF. All animal procedures were approved by the University of Rochester's Committee on Animal Resources.

METHOD DETAILS

Transplantation

Shiverer x Rag2 null and Rag1 null neonatal mice were transplanted on postnatal day 1 or 2. Half of the litter was removed from the dam and placed in a humidified warming chamber. For this we used a sterilized plastic box, lined with sterile gauze dampened with Hanks balanced salt solution, and warmed on a heating block. The pups to be injected were then wiped with Povidone-Iodine and wrapped in sterile gauze to prevent direct contact with ice, then cryo-anesthetized for 2 to 6 min, depending on size. The pups were then removed from ice and cleaned with an alcohol prep pad, then laid in a customized neonatal mouse holder made of baked molded clay. The pups were injected directly through the skin and skull osteoid into both the rostral (at Bregma, ML ± 1.0 mm, ventral 1.0 mm) and caudal (AP −1.0, ML ± 1.0 mm, ventral 0.9 mm) corpus callosum. Following injections, pups were cleaned with alcohol prep pads and returned to the warming chamber for recovery. Upon recovery, the first half of the litter was returned to the dam, and the second half put in the humidified chamber. Pups were weaned between 21 and 28 days, then group housed.

Immunolabeling of tissue sections

Brains were cryopreserved, embedded in OCT (Tissue-Tek OCT, Sakura Finetek, Torrance, CA) and sectioned at 20 μm, either sagittally or coronally, on a cryostat. Human cells were identified with mouse antihuman nuclei, clone 235-1 at 1:800 (MAB1281, EMD Millipore, Billerica, MA). Myelin basic protein was labeled with rat anti-MBP at 1:25 (Ab7349, Abcam, Cambridge, MA), oligodendrocyte progenitors with anti-human-specific PDGFRα (D13C6, XP® rabbit mAb 5241, 1:300, Cell Signaling Tech), oligodendrocytes with mouse anti-human-specific transferrin (clone HT1/13.6.3, 08691231, MP Biomedicals), astrocytes with anti-human-specific GFAP (SMI 21 at 1:1000, Covance, Princeton, NJ). Alexa Fluor secondary antibodies, goat anti- mouse, rat, and rabbit 488, 568, 594, and 647 were used at 1:400 (Life Technologies, Carlsbad, CA).

Antibodies and dilutions used See Key Resources Table.

Western blots

GPCs derived from CWRU22 and CWRU51 were sorted by FACS for CD140a at DIV160-200, directly into cell lysis buffer (NP40, Invitrogen, FNN0021) with protease inhibitor (Roche, 183617025) on ice. The insoluble fraction was removed by centrifugation at 12,000 g for 5 min at 4°C, and the supernatant analyzed for total protein with BCA™ Protein Assay Kit (Thermo, 23227). 10 μg sample aliquots were separated on 4%–12% gradient gels by SDS-PAGE electrophoresis (XCell SureLock, Invitrogen, 071210). Separated protein was transferred to PVDF membranes, which were blocked with 5% dry milk and incubated sequentially with a rabbit polyclonal anti-neurexin-1 antisera (Millipore, ABN161-1, 1:1000) at 4°C overnight, then washed and followed serially by a mouse monoclonal anti-β actin (Abcam, ab173838, 1:5000) at RT for 1h, and anti-mouse and anti-rabbit secondary antibodies (GE Healthcare, 95107-322 and 95107-328, 1:10000) at RT for 1h. Membranes were visualized by chemiluminescence (Mix ECL™ Reagent, GE Healthcare, RPN2236) through exposure of X-ray film. Experiments were repeated 3 times, with 3 different sets of cells.

Behavior

Behavioral tests were scored using either ANY-maze (Stoelting, Wood Dale, IL) or EthoVision (Noldus). Behavioral testing began at either 25 weeks (for pre-pulse inhibition) or 30-36 weeks (all other tests), and typically lasted 3 weeks; starting age was matched between experimentals and controls. A total of 6-12 recipient mice were engrafted and tested per cell line, or 17-36 mice per group for each behavioral comparison, with a roughly equal balance of male (M) and female (F) recipients. All behavioral tests were done by experimenters blinded as to the treatment condition and implanted cell line.

Tests were performed in the same sequence for all mice, and included: *1) Elevated Plus Maze* Each test mouse was placed in the center of a raised, plus-shaped apparatus, consisting of 2 enclosed arms and 2 open arms, facing an open arm (Walf and Frye, 2007). Each tested mouse was videotaped and scored for time spent in the open versus closed arms. *2) Three chamber social choice* The test apparatus is a plexiglass enclosure divided into thirds with connecting doors (Ugo Basile, Italy) (Yang et al., 2011). Each test mouse was first acclimated to the central chamber or 5 min. The doors to the outer chambers were then removed, and the test mouse allowed to explore all three chambers for 10 min. The test mouse was then guided back to the central chamber, and a same sex and age stranger mouse was placed in a cylindrical container in one side chamber, while an empty cylindrical container was placed in the opposite side chamber. The mouse was then recorded for 10 min, and scored with respect to the amount of time it spent with the

stranger mouse versus the empty compartment. 3) *Novel Object Recognition* Each test mouse was placed in an empty 1 ft^2 testing chamber for 5 min to acclimate, then removed, and two identical objects were placed in the chamber. The mouse was returned to the chamber with the objects, placed facing directly away from them, recorded for 10 min and scored for time spent in proximity to each object (Bevins and Besheer, 2006). After one hour, the experiment was repeated, with one of the two objects replaced by a novel object. 4) *Pre-pulse inhibition* Each mouse was placed in a restraint chamber inside a larger isolation cabinet, equipped with sound, light, and air puff generators (SR-LAB, San Diego Instruments), and auditory PPI assessed as described (Geyer and Swerdlow, 2001). 5) *Sucrose preference* This experiment was always performed last, as mice were individually housed in order to measure liquid consumption. Sucrose preference was determined by the percentage of sucrose water consumed as a proportion of all water consumed (Willner et al., 1987). Water is delivered in our colony by Hydropac (Lab Products, Inc.), so an additional Hydropac containing sucrose water was added to the cage and the two packs were weighed daily.

Activity and sleep assessment

Individually-housed mice were video recorded in 12'' x 12'' x 13.5'' acrylic chambers, using infra-red cameras during the dark phase, for 72 continuous hours under 12/12 light/dark conditions. The distance traveled in meters per hour was calculated by Noldus Ethovision software, and averaged across 8 CTRL mice (gray fill, lines 22 and 17) and 10 SCZ mice (purple fill, line 52). In addition, transitions between phases of the light cycle (measured 30 min before and 30 min after light changes) were analyzed in terms of the number of consecutive seconds of immobility as a percentage of total immobility (AnyMaze, Stoelting), per 30 min measurement block as described (McShane et al., 2010; Pack et al., 2007).

RNA-seq

hGPCs assessed for gene expression were first sorted by fluorescence-activated cell sorting on the basis of the cell surface marker CD140a (BD PharMingen) as described (Sim et al., 2011) (Figure S2). Using polyA-selection, mRNA was isolated from these PDGFRα^+ hGPCs, which were derived from iPSCs made from 4 patients with juvenile-onset schizophrenia (SCZ line numbers 8 [n = 4 independent cell preparations], 29 [n = 3], 51 [n = 7], and 164 [n = 8]); and 3 demographically similar healthy controls (CTR lines 22 [n = 3], 37 [n = 4], and 205 [n = 7]). Sequencing libraries were prepared using the TruSeq RNA v2 kit, and sequenced on an Illumina HiSeq 2500 platform for approximately 45 million 1x100 bp reads per sample. The sequencing reads were pre-processed by trimming off adaptor and low-quality sequences from the 3′ end using Trimmomatic (Bolger et al., 2014). The quality of reads before and after pre-processing was assessed with FastQC (D'Antonio et al., 2015), and the pre-processed reads were then aligned to the RefSeq NCBI reference human genome version GRCh38 (Pruitt et al., 2007) with Subread read aligner (Liao et al., 2013) using Hamming distance to break ties between more than one optimal mapping locations. Raw gene counts were obtained from BAM alignment files with the featureCounts tool (Liao et al., 2014).

For bioinformatic analysis, see Quantification and Statistical Analysis section below.

QUANTIFICATION AND STATISTICAL ANALYSIS

Imaging and quantitative histology

For mapping the distribution of human nuclei, or photographing gross distribution of myelin at low power, whole brain sections were imaged on a Leica LMD 6500. Imaging for phenotypic counts was performed on an Olympus BX51 driven by Stereo Investigator software (MBF, Williston, VT).

Astrocyte morphometrics

Shiverer x rag2 null mice were sacrificed at 4.5 months of age and their white matter astrocyte morphologies assessed. 150 μm thick coronal slices were taken by Vibratome at Bregma −1.0 mm from control (22, 37 and C27) or SCZ (51, 164, 193) hGPC-engrafted mice, incubated in mouse anti-hGFAP for 1 week, then 4 hr in Alexa 568 goat anti-mouse. The slices were mounted on slides and imaged at 100x by confocal (Leica SP8). The images were traced using Neurolucida 360 (MicroBrightfield, Inc.); all tracings were done by experimenters blinded as to the treatment condition.

Individual astrocytes were selected from the middle of the corpus callosum at mid-depth so as to capture cells and their processes in their entirety. Nine cells/brain were analyzed by Neurolucida with Sholl analysis, as 3 cells/slice and 3 slices/brain, taken at 500, 1000, and 1500 μm lateral of the midline. Two or three brains were assessed for each of three lines produced from separate patients, for a total of 8 brains and 72 traced cells/condition, for both CTRL and SCZ-engrafted groups. For Sholl analysis, concentric shells placed at successively increasing diameters of 5 μm were centered on the cell body, and the number of intersections between cell processes and shells counted (Sholl, 1953). For the assessment and quantitative description of astrocytic fiber 3D architecture, Fan-in analysis (MBF Biosciences) was used as previously described for studies of dendritic topology (Dang et al., 2014).

Myelin luminance analysis

To measure forebrain myelination, we used luminance analysis based on measurement of myelin basic protein (MBP) immunofluorescence. Evenly-spaced and uniformly sampled coronal sections were stained for MBP as described, and images taken at 10x using a Nikon Ni-E and Nikon DS-Fi1 camera. The corpus callosum was selected as region of interest, and mean intensity values were obtained using NIS Elements v.4.5.

Statistical analysis

Unless otherwise noted, all analyses were done in GraphPad Prism v.7. Individual tests were performed as noted for each experiment; all data shown as Means ± SEM.

Bioinformatics

Raw RNaseq gene counts were obtained as noted above. After eliminating lowly expressed transcripts with < 5 reads in more than 5 samples across the dataset, the count data was normalized using the RUVSeq (Risso et al., 2014) R Bioconductor package (Gentleman et al., 2004) to account for variance. As described in the RUVSeq manual, the normalization was accomplished in the following three-step procedure: 1) in silico negative control genes were determined by first-pass differential expression analysis by the edgeR (Robinson et al., 2010) and DESeq2 (Love et al., 2014) R Bioconductor packages, taking genes with FDR-adjusted P values > 0.75, as calculated by both methods (approximately 7000 genes were unaffected by the condition of interest); 2) the negative control genes were then used in the RUVs function of the RUVSeq package, for calculation of variance factors; and, 3) the second-pass differential expression analysis (5% FDR and log2 fold change > 1) for determining disease-dysregulated genes was performed using the original counts, adjusting for RUVs-calculated variance factors by multi-factor GLM models implemented in the edgeR and DESeq2 packages.

This three-step analysis, with filtering for low-expressed transcripts, was used to compare each SCZ-derived hGPC cell line to the pooled CTR-derived hGPCs. The intersection of the resulting 4 individual lists of differentially expressed genes was taken as the conserved representative list of SCZ-dysregulated genes. In the normalization procedure for each comparison, the number of RUVs-calculated variance factors was limited to 1 for line 29, 3 for lines 8 and 164, and 7 for line 51, as determined by principal component and hierarchical clustering analyses performed with native R functions (https://www.R-project.org). To obtain average fold changes and P values for dysregulated genes in all 4 SCZ hGPC lines, a differential expression comparison of pooled SCZ to pooled CTR lines was performed by the same filtering and analysis workflow with the number of variance factors limited to 9.

For all differential expression comparisons, only the significant results that agreed between edgeR and DESeq2 methods were used in downstream analysis. Once individual fold changes and P values for dysregulated genes in all 4 SCZ hGPC lines were established relative to control lines, the differential expression of pooled SCZ to pooled CTR lines was performed. For each SCZ cell line, separate DE comparisons were performed against each control line and the intersection of the DE genes was taken as a representative list for that SCZ line against the control population. Fold changes and FDR-adjusted P values reported were calculated by edgeR. Functional annotation of the conserved set of SCZ-dysregulated genes was done using ToppCluster (Kaimal et al., 2010) and Ingenuity Pathway Analysis (IPA) (http://www.qiagen.com/ingenuity). Network visualization and analysis of the results of functional annotation were performed in Gephi (Jacomy et al., 2014) visualization software.

Real-Time PCR

Expression levels in SCZ- and control derived GPCs of selected target genes identified by RNA-seq were assayed by TaqMan Low Density Array (TLDA) Real-Time PCR. The raw data were analyzed in EspressionSuite Software version 1.1 supplied by Applied Biosystems and exported into HTqPCR R package *(27)* for relative quantification analysis.

DATA AND SOFTWARE AVAILABILITY

For streamlined execution of the above data processing and analysis routines, a set of Python and R scripts was developed. The code and the data files needed to reproduce our normalization and differential expression pipeline are available from https://github.com/cbtncph/GoldmanetalSCZ2016.

All genomic data have been deposited to GEO: GSE86906.

Cell Stem Cell, Volume *21*

Supplemental Information

Human iPSC Glial Mouse Chimeras Reveal Glial Contributions to Schizophrenia

Martha S. Windrem, Mikhail Osipovitch, Zhengshan Liu, Janna Bates, Devin Chandler-Militello, Lisa Zou, Jared Munir, Steven Schanz, Katherine McCoy, Robert H. Miller, Su Wang, Maiken Nedergaard, Robert L. Findling, Paul J. Tesar, and Steven A. Goldman

Supplementary Materials

Human iPSC glial mouse chimeras reveal glial contributions to schizophrenia

Martha S. Windrem[1], Mikhail Osipovitch[2], Zhengshan Liu[1], Janna Bates[1], Devin Chandler-Militello[1], Lisa Zou[1], Jared Munir[1], Steven Schanz[1], Katherine McCoy[1], Robert H. Miller[3], Su Wang[1], Maiken Nedergaard[1,2], Robert L. Findling[4], Paul J. Tesar[5], Steven A. Goldman[1,2*]

Correspondence to: steven_goldman@urmc.rochester.edu or goldman@sund.ku.dk

This PDF file includes:

Figures S1 to S5

Tables S1 to S3

SUPPLEMENTARY FIGURES

Figure S1 *(related to Figures 1, 2 and 4)*

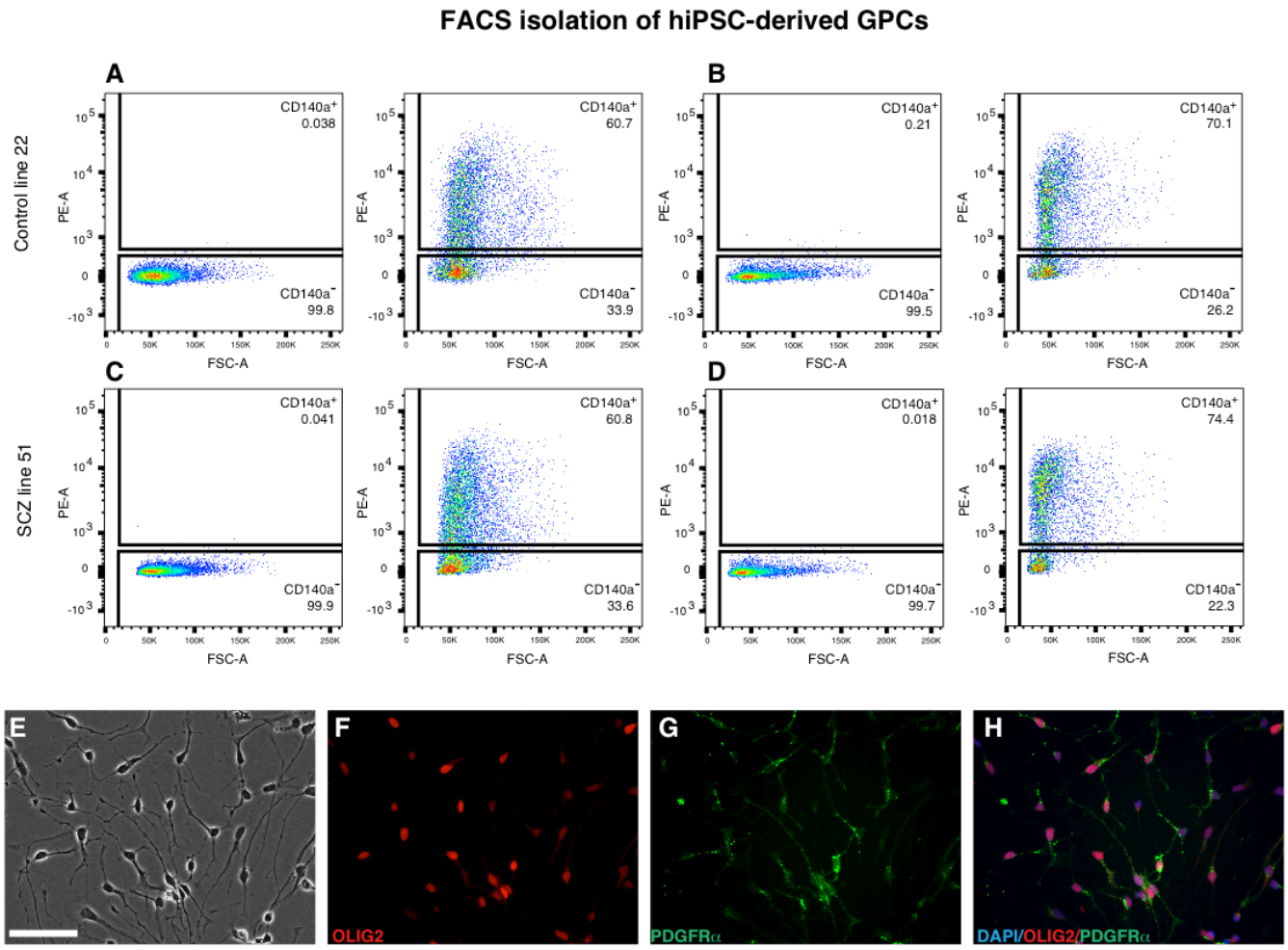

Figure S1

CD140a$^+$ glial progenitor cells could be efficiently produced from both SCZ and normal hiPSCs

Flow cytometry for CD140a/PDGFαR$^+$ glial progenitor cells (*right* plots, compared to unstained gating controls on *left*), reveals dominant proportions of CD140a-defined cells in both normal control patient-derived (*top*, **A-B**) and SCZ-derived (*bottom,* **C-D**) preparations. **A-C** and **B-D** were run as matched pairs; **A** and **C**, 177 and 168 days in vitro (DIV); **B** and **D**, 188 and 196 DIV. **E-H** show a representative post-FACS preparation of CD140a-sorted cells, as **E**, a phase image, immunostained for both olig2 (**F**, *red*) and PDGFRα (**G; H**, *merged*). These plots were typical of GPC cultures of both normal and SCZ-derived hiPSC lines. The sorted populations were used for genomics assessment, while both sorted and unsorted cells were used for transplantation, with no evident performance differences between the two.

Figure S2 *(related to Figure 2)*

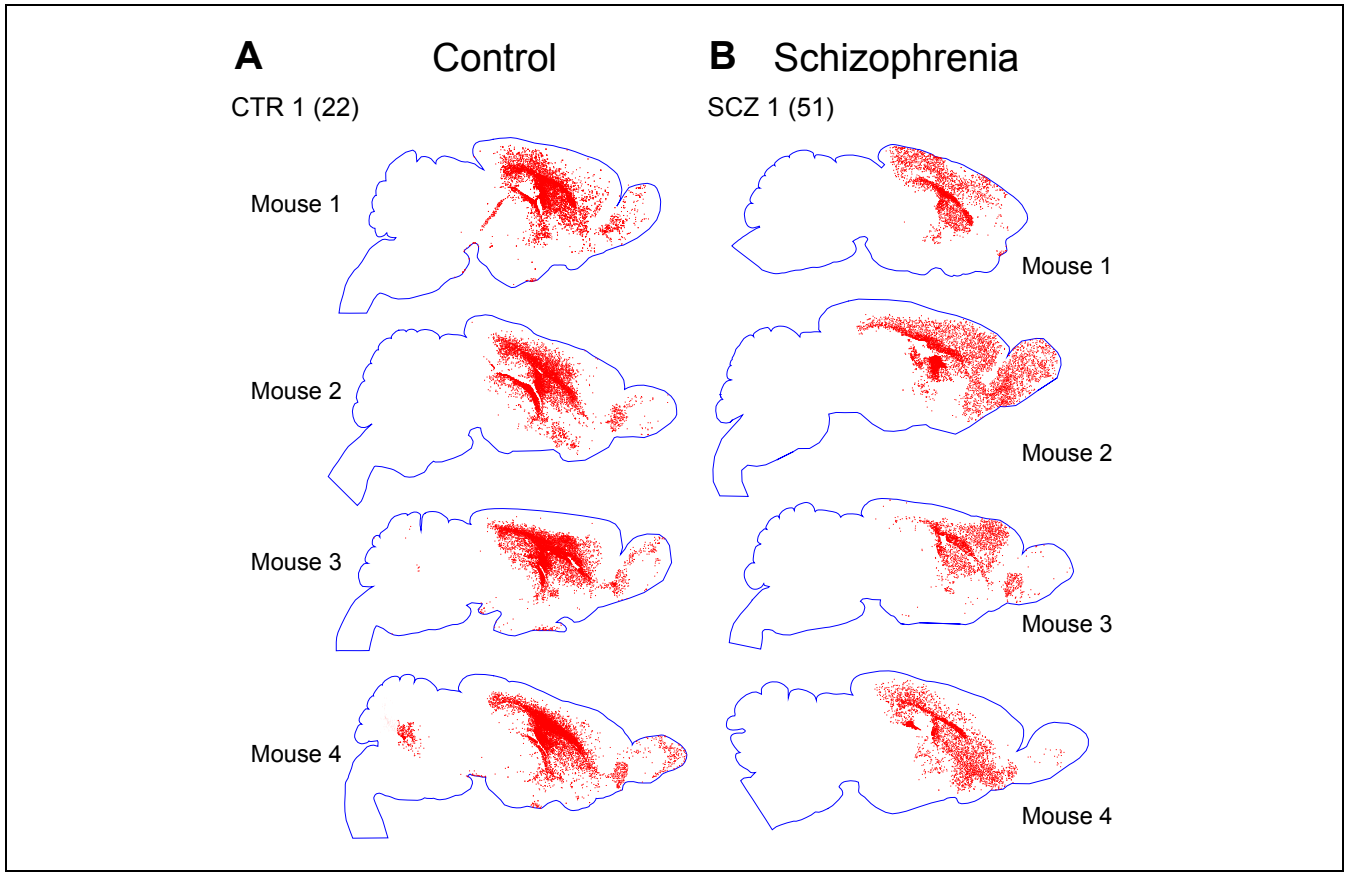

Figure S2

Schizophrenia-derived GPCs exhibit aberrant dispersal in vivo

The dispersal patterns of GPCs produced from SCZ patients typically differed from that of iPSC hGPCs derived from normal patients, in that SCZ GPCs did not remain and expand within the white matter before progressing to cortical infiltration, as was otherwise invariably the case with normal GPCs. A-B show 4 mice each implanted with either control subject-derived (line 22) or SCZ patient-derived (line 51) hGPCs. All SCZ hGPC-engrafted mice show disproportionate hGPC entry into the cortical and striatal gray matter, with less expansion and hence less net engraftment in the forebrain white matter tracts. This difference in hGPC dispersal pattern was noted consistently in all 4 SCZ lines assessed in vivo, each derived from a different patient, relative to their matched 4 control lines, similarly obtained from distinct patients (see **Figure 2**).

Figure S3 *(related to Figure 4)*

Heat maps of significantly dysregulated genes in schizophrenic relative to control hiPSC GPCs

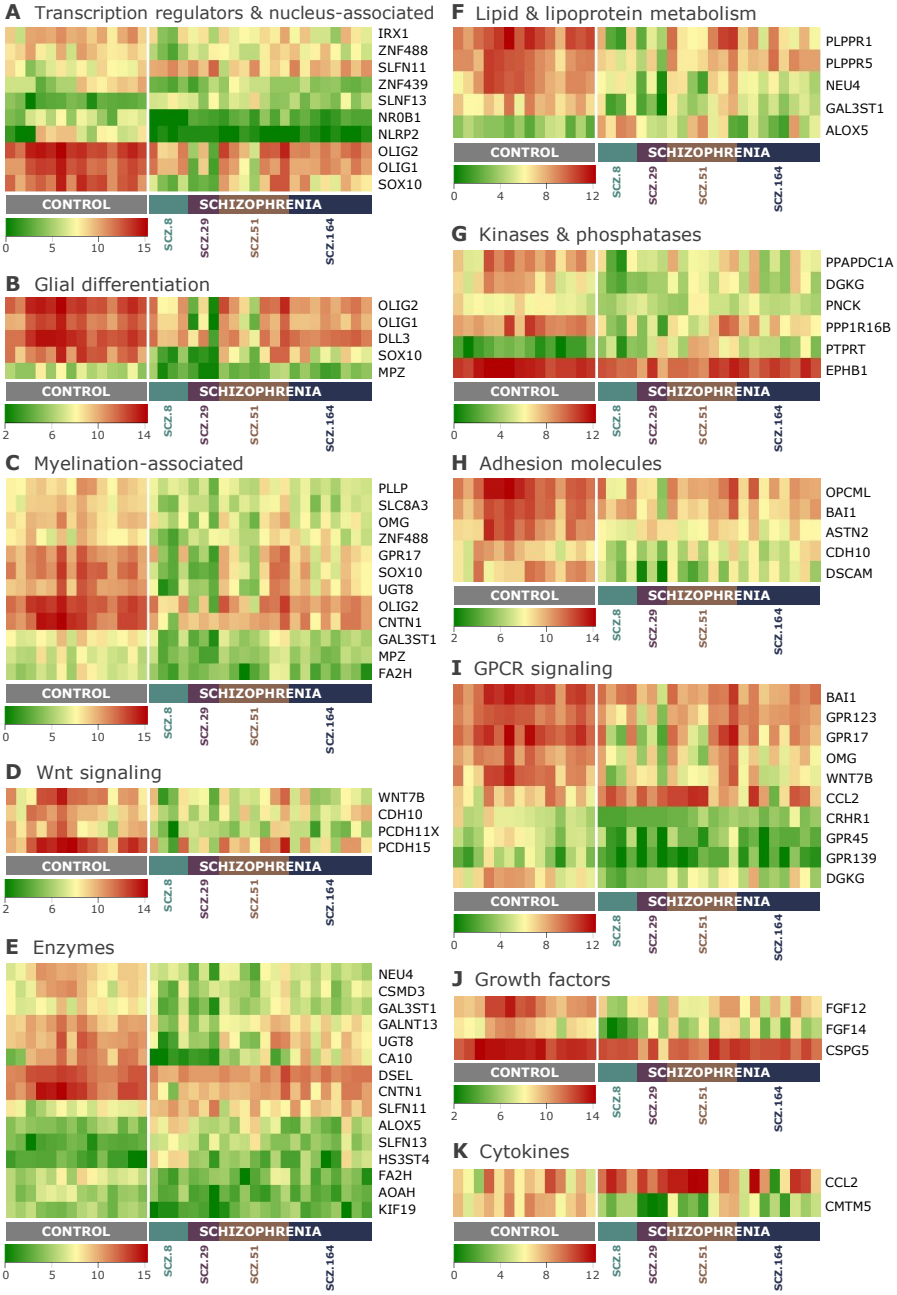

Expression patterns for shared genes differentially expressed by hiPSC GPCs derived from 4 schizophrenic patients, relative to the pooled gene expression pattern of hGPCs derived from 3 control-derived iPSCs (log2 fold change >1.0, FDR 5%, 118 genes total). The dysregulated genes were manually annotated and grouped into relevant sets based on their function and cellular localization. Each heat map visualizes UQ-normalized, log2-transformed counts of genes grouped into the following functional categories, comprising genes encoding: **(A)** transcription regulators, zinc finger proteins, and other nucleus-associated proteins; **(B)** glial differentiation-associated proteins; **(C)** myelin-related genes and transcription factors; **(D)** Wnt pathway effectors; **(E)** metabolic enzymes; **(F)** lipid and lipoprotein metabolism; **(G)** kinases and phosphatases; **(H)** adhesion molecules, cadherins; and astrotactins; **(I)** GPCR signal intermediates; **(J)** growth factors; and **(K)** cytokines.

Figure S4 *(related to Figure 4)*

Additional heat maps of significantly dysregulated genes in SCZ relative to control hGPCs

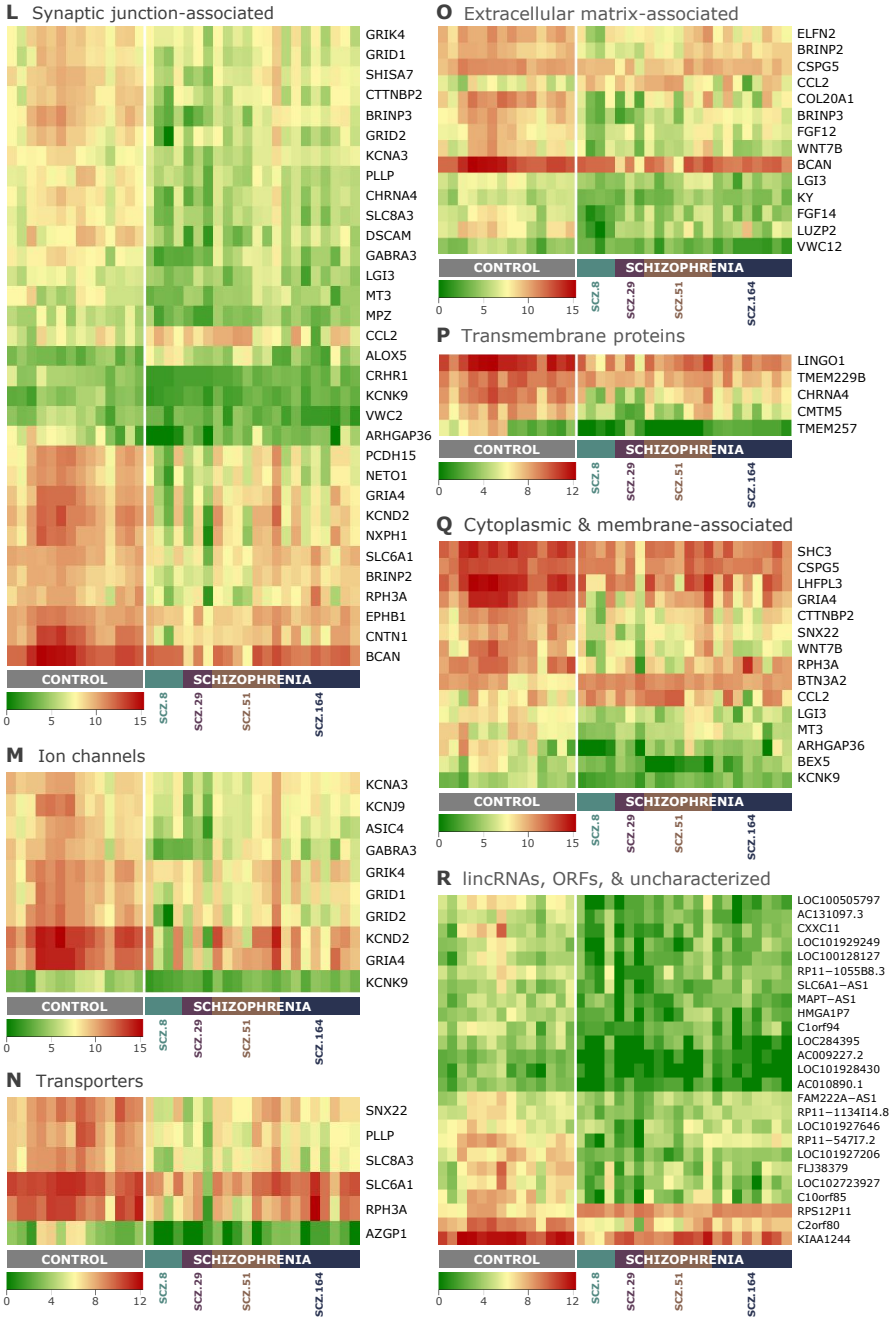

Additional heat maps of significantly dysregulated genes in SCZ relative to control hGPCs

As in **Figure S3**, expression patterns for genes differentially expressed by hiPSC GPCs derived from 4 SCZ patients, relative to the pooled gene expression pattern of hGPCs derived from 3 control-derived iPSCs (log2-fold change >1.0, FDR 5%, 118 genes total). As in **Figure S3**, which is derived from the same data set, each heat map visualizes UQ-normalized, log2-transformed counts of differentially expressed genes. These are grouped into the following functional categories, which follow those listed in **Figure S3**: **(L)** cell signaling and synaptic proteins; **(M)** ion channels; **(N)** transporters; **(O)** extracellular matrix constituents; **(P)** other transmembrane proteins; **(Q)** other cytoplasmic and membrane-bound proteins; and **(R)** unannotated genes, open reading frames, and long intergenic non-coding RNAs.

Figure S5 *(related to Figure 5)*

Neurexin-1 expression was suppressed in SCZ hiPSC GPCs

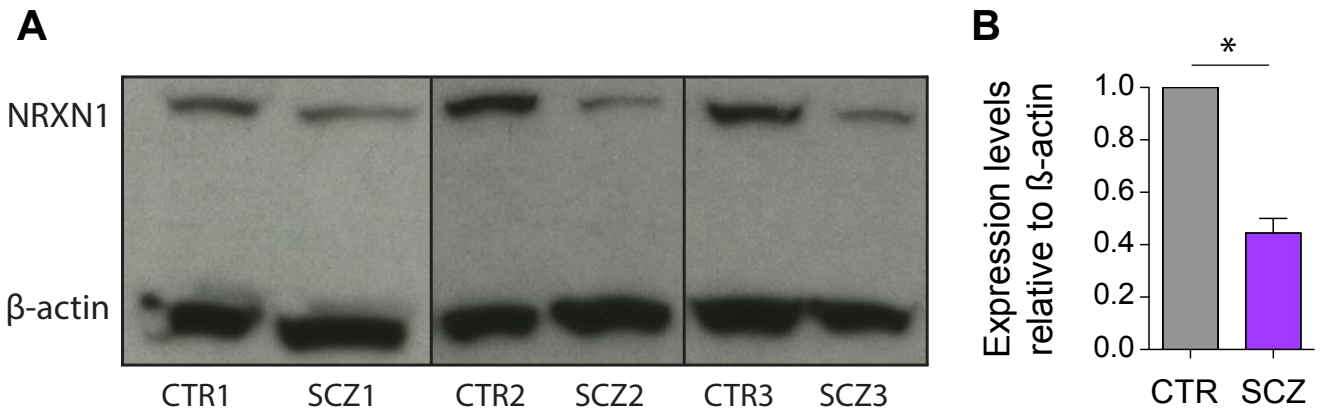

A, Western blots revealed that neurexin-1 protein was abundantly expressed by human GPCs purified by CD140a-directed FACS, and that neurexin-1 levels were lower in otherwise matched SCZ hGPCs (line 51 SCZ hGPCs vs. line 22 CTRL hGPCs). **B,** Quantitative densitometry revealed the significant decrease in neurexin1 protein expression by SCZ hGPCs relative to their CTR hGPCs. *p<0.05, Student's t-test.

SUPPLEMENTARY TABLES

Table S1 (*related to Figure 1*)

Patients and cell lines used in this study

Subject number	hiPSC Line(s)	Age of subject	Gender	Ethnicity	RNA-Seq of CD140a^{+} GPCs	Anatomic assessment N=shiverer mice	Behavioral assessment N=myelin w/t mice
	Control Subjects						
Cntrl 1	**19, 22**	26	M	C	√	√	√
Cntrl 2	**37**	32	F	AA	√	√	√
Cntrl 3	**205**	25	M	C	√	√	√
Cntrl 4	**C27**	NA	NA	NA	√	√	
	Schizophrenic Subjects						
SCZ 1	**8**	10	F	C	√	√	
SCZ 2	**51, 52**	16	M	C	√	√	√
SCZ 3	**29, 31**	12	M	C	√		√
SCZ 4	**164**	14	F	AA	√	√	
SCZ 5	**193**	15	F	NA		√	√

A total of 11 new independent iPS cell lines were derived from 8 subjects; 5 juvenile-onset schizophrenic patients and 3 healthy controls; an established control line (C27) from an additional normal subject was published previously (Chambers et al., 2009; Wang et al., 2013), and graciously provided by L. Studer. hGPCs derived from these cells were assigned to individual experiments as noted. C, Caucasian; AA, African-American; NA, not available.

Table S2 (*related to Figure 4*)

Significantly dysregulated genes in schizophrenic relative to control GPCs

These tables list shared genes differentially expressed by hiPSC GPCs derived from 4 SCZ patients, relative to the pooled gene expression pattern of hGPCs from 3 control-derived iPSCs (log2 fold change >1.0, FDR 5%, 116 genes total, *red*, upregulated in SCZ vs CTRL; *green*, downregulated in SCZ GPCs). The fold- changes (FC) and FDR-adjusted *p* values shown here were derived from the comparison of the pooled SCZ-derived GPC lines to the pooled control-derived GPC lines. Dysregulated genes were grouped into functional sets by their cellular roles and localizations.

Gene ID	*Log2 FC*	*P Value*	*Entrez Gene Name*
Transcription regulators, & nucleus-associated (10 genes)			
SLFN13	2.832	2.18E-13	schlafen family member 13
SLFN11	2.193	6.47E-09	schlafen family member 11
NLRP2	-7.208	4.24E-58	NLR family, pyrin domain containing 2
SOX10	-4.448	8.37E-19	SRY-box 10
NR0B1	-3.321	5.92E-27	nuclear receptor subfamily 0 group B member 1
OLIG2	-3.196	4.23E-19	oligodendrocyte lineage transcription factor 2
OLIG1	-3.146	5.72E-22	oligodendrocyte transcription factor 1
ZNF439	-2.139	6.14E-08	zinc finger protein 439
IRX1	-1.815	5.52E-06	iroquois homeobox 1
ZNF488	-1.464	4.44E-07	zinc finger protein 488
Glial differentiation (5 genes)			
SOX10	-4.448	8.37E-19	SRY-box 10
OLIG2	-3.196	4.23E-19	oligodendrocyte lineage transcription factor 2
OLIG1	-3.146	5.72E-22	oligodendrocyte transcription factor 1
DLL3	-2.352	2.09E-24	delta-like 3 (Drosophila)
MPZ	-2.105	7.66E-13	myelin protein zero
Myelination-associated (12 genes)			
SOX10	-4.448	8.37E-19	SRY-box 10
GPR17	-3.357	1.94E-10	G protein-coupled receptor 17
UGT8	-3.250	4.36E-09	UDP glycosyltransferase 8
OLIG2	-3.196	4.23E-19	oligodendrocyte lineage transcription factor 2
GAL3ST1	-2.681	4.01E-12	galactose-3-O-sulfotransferase 1
CNTN1	-2.675	5.65E-15	contactin 1
PLLP	-2.581	1.21E-24	plasmolipin
OMG	-2.561	5.09E-12	oligodendrocyte myelin glycoprotein
FA2H	-2.440	4.45E-08	fatty acid 2-hydroxylase
SLC8A3	-2.224	2.00E-12	solute carrier family 8 (sodium/calcium exchanger), member 3
MPZ	-2.105	7.66E-13	myelin protein zero
ZNF488	-1.464	4.44E-07	zinc finger protein 488
Wnt signaling (4 genes)			
WNT7B	-2.626	1.46E-07	wingless-type MMTV integration site family member 7B
PCDH15	-2.530	1.42E-10	protocadherin-related 15
PCDH11X	-2.364	1.25E-08	protocadherin 11 X-linked
CDH10	-1.646	9.33E-07	cadherin 10
Enzymes (15 genes)			
SLFN13	2.832	2.18E-13	schlafen family member 13
SLFN11	2.193	6.47E-09	schlafen family member 11
HS3ST4	2.149	1.44E-04	heparan sulfate-glucosamine 3-sulfotransferase 4
ALOX5	1.777	2.35E-05	arachidonate 5-lipoxygenase
CA10	-3.550	3.07E-08	carbonic anhydrase X
NEU4	-3.361	8.31E-40	neuraminidase 4 (sialidase)
UGT8	-3.250	4.36E-09	UDP glycosyltransferase 8
GAL3ST1	-2.681	4.01E-12	galactose-3-O-sulfotransferase 1
CNTN1	-2.675	5.65E-15	contactin 1
CSMD3	-2.560	5.78E-10	CUB and Sushi multiple domains 3
GALNT13	-2.467	2.80E-11	polypeptide N-acetylgalactosaminyltransferase 13
FA2H	-2.440	4.45E-08	fatty acid 2-hydroxylase
AOAH	-2.271	2.99E-12	acyloxyacyl hydrolase
KIF19	-1.644	5.10E-06	kinesin family member 19
DSEL	-1.151	1.35E-10	dermatan sulfate epimerase-like
Lipid & lipoprotein metabolism (5 genes)			
ALOX5	1.777	2.35E-05	arachidonate 5-lipoxygenase
NEU4	-3.361	8.31E-40	neuraminidase 4 (sialidase)
GAL3ST1	-2.681	4.01E-12	galactose-3-O-sulfotransferase 1
PLPPR1	-2.652	1.16E-09	phospholipid phosphatase related 1
PLPPR5	-1.573	1.69E-09	phospholipid phosphatase related 5

Kinases & phosphatases (6 genes)

PTPRT	4.410	1.69E-17	protein tyrosine phosphatase, receptor type T
PPP1R16B	-2.665	1.29E-09	protein phosphatase 1 regulatory subunit 16B
PPAPDC1A	-2.357	6.76E-09	phospholipid phosphatase 4
DGKG	-2.306	9.29E-12	diacylglycerol kinase gamma
EPHB1	-1.344	3.89E-17	EPH receptor B1
PNCK	-1.226	4.25E-08	pregnancy up-regulated nonubiquitous CaM kinase

Adhesion molecules (5 genes)

DSCAM	-3.148	1.58E-12	Down syndrome cell adhesion molecule
ASTN2	-2.242	4.70E-21	astrotactin 2
OPCML	-2.099	7.87E-10	opioid binding protein/cell adhesion molecule-like
BAI1	-2.000	1.31E-12	adhesion G protein-coupled receptor B1
CDH10	-1.646	9.33E-07	cadherin 10

GPCR signaling (10 genes)

CCL2	1.832	1.97E-07	chemokine (C-C motif) ligand 2
GPR17	-3.357	1.94E-10	G protein-coupled receptor 17
GPR45	-2.895	2.95E-14	G protein-coupled receptor 45
WNT7B	-2.626	1.46E-07	wingless-type MMTV integration site family member 7B
GPR139	-2.589	1.32E-08	G protein-coupled receptor 139
OMG	-2.561	5.09E-12	oligodendrocyte myelin glycoprotein
CRHR1	-2.382	5.81E-12	corticotropin releasing hormone receptor 1
DGKG	-2.306	9.29E-12	diacylglycerol kinase gamma
BAI1	-2.000	1.31E-12	adhesion G protein-coupled receptor B1
GPR123	-1.807	1.76E-18	adhesion G protein-coupled receptor A1

Growth factors (3 genes)

FGF14	-2.021	5.14E-07	fibroblast growth factor 14
FGF12	-1.988	5.47E-09	fibroblast growth factor 12
CSPG5	-1.285	6.38E-17	chondroitin sulfate proteoglycan 5

Cytokines (2 genes)

CCL2	1.832	1.97E-07	chemokine (C-C motif) ligand 2
CMTM5	-3.023	3.69E-15	CKLF-like MARVEL transmembrane domain containing 5

Synaptic-junction associated (32 genes)

CCL2	1.832	1.97E-07	chemokine (C-C motif) ligand 2
ALOX5	1.777	2.35E-05	arachidonate 5-lipoxygenase
BRINP3	-3.433	4.70E-22	bone morphogenetic protein/retinoic acid inducible neural-specific 3
DSCAM	-3.148	1.58E-12	Down syndrome cell adhesion molecule
KCND2	-3.145	5.67E-11	potassium channel, voltage gated Shal related subfamily D, member 2
NXPH1	-2.892	3.11E-15	neurexophilin 1
CHRNA4	-2.755	4.45E-14	cholinergic receptor, nicotinic alpha 4
ARHGAP36	-2.686	1.21E-05	Rho GTPase activating protein 36
CNTN1	-2.675	5.65E-15	contactin 1
NETO1	-2.633	2.52E-12	neuropilin and tolloid like 1
PLLP	-2.581	1.21E-24	plasmolipin
PCDH15	-2.530	1.42E-10	protocadherin-related 15
GRIA4	-2.519	1.84E-09	glutamate receptor, ionotropic, AMPA 4
BCAN	-2.473	7.35E-32	brevican
GABRA3	-2.450	1.08E-12	gamma-aminobutyric acid (GABA) A receptor, alpha 3
CRHR1	-2.382	5.81E-12	corticotropin releasing hormone receptor 1
SHISA7	-2.302	1.43E-14	shisa family member 7
SLC8A3	-2.224	2.00E-12	solute carrier family 8 (sodium/calcium exchanger), member 3
MPZ	-2.105	7.66E-13	myelin protein zero
GRID2	-2.055	3.65E-06	glutamate receptor, ionotropic, delta 2
RPH3A	-2.014	1.01E-06	rabphilin 3A
VWC2	-2.003	9.67E-13	von Willebrand factor C domain containing 2
CTTNBP2	-1.904	7.21E-08	cortactin binding protein 2
MT3	-1.795	5.27E-09	metallothionein 3
KCNA3	-1.719	3.03E-12	potassium channel, voltage gated shaker related subfamily A, member 3
BRINP2	-1.625	2.03E-12	bone morphogenetic protein/retinoic acid inducible neural-specific 2
LGI3	-1.614	4.07E-08	leucine-rich repeat LGI family member 3
SLC6A1	-1.596	5.52E-11	solute carrier family 6 (neurotransmitter transporter), member 1
GRID1	-1.562	7.61E-07	glutamate receptor, ionotropic, delta 1
GRIK4	-1.547	2.73E-07	glutamate receptor, ionotropic, kainate 4
KCNK9	-1.460	4.40E-06	potassium channel, two pore domain subfamily K, member 9
EPHB1	-1.344	3.89E-17	EPH receptor B1

Ion channels (10 genes)

KCND2	-3.145	5.67E-11	potassium channel, voltage gated Shal related subfamily D, member 2
GRIA4	-2.519	1.84E-09	glutamate receptor, ionotropic, AMPA 4
GABRA3	-2.450	1.08E-12	gamma-aminobutyric acid (GABA) A receptor, alpha 3
ASIC4	-2.321	4.13E-14	acid sensing ion channel subunit family member 4
KCNJ9	-2.187	2.85E-21	potassium channel, inwardly rectifying subfamily J, member 9
GRID2	-2.055	3.65E-06	glutamate receptor, ionotropic, delta 2
KCNA3	-1.719	3.03E-12	potassium channel, voltage gated shaker related subfamily A, member 3
GRID1	-1.562	7.61E-07	glutamate receptor, ionotropic, delta 1
GRIK4	-1.547	2.73E-07	glutamate receptor, ionotropic, kainate 4
KCNK9	-1.460	4.40E-06	potassium channel, two pore domain subfamily K, member 9

Transporters (6 genes)

AZGP1	-3.323	1.66E-08	alpha-2-glycoprotein 1, zinc-binding
PLLP	-2.581	1.21E-24	plasmolipin
SNX22	-2.297	3.53E-20	sorting nexin 22
SLC8A3	-2.224	2.00E-12	solute carrier family 8 (sodium/calcium exchanger), member 3
RPH3A	-2.014	1.01E-06	rabphilin 3A
SLC6A1	-1.596	5.52E-11	solute carrier family 6 (neurotransmitter transporter), member 1

Extracellular matrix-associated (14 genes)

CCL2	1.832	1.97E-07	chemokine (C-C motif) ligand 2
COL20A1	-3.476	7.33E-14	collagen, type XX, alpha 1
BRINP3	-3.433	4.70E-22	bone morphogenetic protein/retinoic acid inducible neural-specific 3
WNT7B	-2.626	1.46E-07	wingless-type MMTV integration site family member 7B
BCAN	-2.473	7.35E-32	brevican
FGF14	-2.021	5.14E-07	fibroblast growth factor 14
VWC2	-2.003	9.67E-13	von Willebrand factor C domain containing 2
FGF12	-1.988	5.47E-09	fibroblast growth factor 12
LUZP2	-1.948	7.22E-06	leucine zipper protein 2
ELFN2	-1.943	1.47E-06	extracellular Leu-rich repeat and fibronectin type III domain containing 2
KY	-1.873	2.41E-13	kyphoscoliosis peptidase
BRINP2	-1.625	2.03E-12	bone morphogenetic protein/retinoic acid inducible neural-specific 2
LGI3	-1.614	4.07E-08	leucine-rich repeat LGI family member 3
CSPG5	-1.285	6.38E-17	chondroitin sulfate proteoglycan 5

Transmembrane proteins (5 genes)

TMEM257	-4.018	5.58E-23	transmembrane protein 257
CMTM5	-3.023	3.69E-15	CKLF-like MARVEL transmembrane domain containing 5
CHRNA4	-2.755	4.45E-14	cholinergic receptor, nicotinic alpha 4
LINGO1	-2.139	3.56E-14	leucine-rich repeat and Ig domain containing 1
TMEM229B	-1.187	7.76E-06	transmembrane protein 229B

Cytoplasmic & membrane-associated (15 genes)

CCL2	1.832	1.97E-07	chemokine (C-C motif) ligand 2
BTN3A2	1.355	8.10E-20	butyrophilin subfamily 3 member A2
BEX5	-3.885	2.55E-21	brain expressed X-linked 5
ARHGAP36	-2.686	1.21E-05	Rho GTPase activating protein 36
WNT7B	-2.626	1.46E-07	wingless-type MMTV integration site family member 7B
GRIA4	-2.519	1.84E-09	glutamate receptor, ionotropic, AMPA 4
SNX22	-2.297	3.53E-20	sorting nexin 22
LHFPL3	-2.250	1.71E-07	lipoma HMGIC fusion partner-like 3
RPH3A	-2.014	1.01E-06	rabphilin 3A
CTTNBP2	-1.904	7.21E-08	cortactin binding protein 2
SHC3	-1.830	7.88E-19	SHC (Src homology 2 domain containing) transforming protein 3
MT3	-1.795	5.27E-09	metallothionein 3
LGI3	-1.614	4.07E-08	leucine-rich repeat LGI family member 3
KCNK9	-1.460	4.40E-06	potassium channel, two pore domain subfamily K, member 9
CSPG5	-1.285	6.38E-17	chondroitin sulfate proteoglycan 5

lincRNAs, ORFs, & uncharacterized (25 genes)

RPS12P11	1.647	9.02E-30	not available
LOC101927206	-3.592	2.74E-63	not available
LOC100505797	-3.266	3.10E-27	myosin heavy chain IB-like
C10orf85	-3.081	3.52E-10	long intergenic non-protein coding RNA 1561
CXXC11	-2.814	7.70E-19	receptor (chemosensory) transporter protein 5 (putative)
LOC284395	-2.792	1.20E-10	uncharacterized LOC284395
RP11-547I7.2	-2.779	4.81E-34	not available
AC009227.2	-2.758	3.05E-13	not available
LOC101928430	-2.691	5.56E-10	not available
FLJ38379	-2.389	1.25E-15	not available
LOC102723927	-2.363	7.74E-21	uncharacterized LOC102723927
RP11-1055B8.3	-2.336	1.02E-16	not available
AC131097.3	-2.180	5.80E-16	not available
C1orf94	-2.077	7.03E-11	chromosome 1 open reading frame 94
HMGA1P7	-2.057	4.49E-09	high mobility group AT-hook 1 pseudogene 7
LOC101929249	-2.003	1.52E-06	uncharacterized LOC101929249
LOC101927646	-2.001	1.22E-10	uncharacterized LOC101927646
AC010890.1	-1.937	3.53E-10	not available
C2orf80	-1.924	6.74E-18	chromosome 2 open reading frame 80
MAPT-AS1	-1.844	5.40E-07	MAPT antisense RNA 1
LOC100128127	-1.814	1.43E-09	not available
RP11-1134I14.8	-1.783	5.72E-22	not available
SLC6A1-AS1	-1.706	1.31E-09	SLC6A1 antisense RNA 1
KIAA1244	-1.643	1.63E-10	ARFGEF family member 3
FAM222A-AS1	-1.297	1.10E-11	FAM222A antisense RNA 1

Table S3 (*related to Figure 5*)

Significantly dysregulated synaptic genes in SCZ GPCs

	SCZ.08 vs. Pooled CTR		*SCZ.29 vs. Pooled CTR*		*SCZ.51 vs. Pooled CTR*		*SCZ.164 vs. Pooled CTR*		*SCZ.08+29+51+164 vs. Pooled CTR*	
Gene ID	*Log2 FC*	*P Value*	*Log2 FC*	*P Value*	*Log2 FC*	*P Value*	*Log2 FC*	*P Value*	*Log2 FC*	*P Value*
DSCAML1	-1.971	8.83E-07	-2.968	1.31E-04	-1.089	8.32E-05	NS	NS	-0.982	5.34E-08
LINGO1	-2.320	3.29E-04	-2.885	2.26E-04	-1.452	3.36E-06	-2.523	9.19E-12	-2.139	3.56E-14
NLGN1	-1.249	3.37E-04	-1.014	4.32E-02	NS	NS	-0.545	3.88E-02	-0.625	3.15E-04
NLGN2	NS	NS	-0.767	1.74E-02	-0.384	3.01E-03	-0.408	1.47E-02	-0.452	3.37E-06
NLGN3	-0.563	3.98E-02	-1.669	3.07E-03	-1.011	1.63E-09	-0.958	3.67E-05	-1.143	1.61E-19
NRP1	-1.362	1.15E-03	1.409	5.00E-04	NS	NS	NS	NS	NS	NS
NRP2	NS	NS	1.548	2.07E-03	NS	NS	-0.733	3.65E-02	NS	NS
NRXN1	-3.259	5.93E-06	-2.984	5.55E-03	-1.176	1.35E-02	NS	NS	-1.161	2.04E-04
NRXN2	NS	NS	-2.179	9.04E-06	-1.252	2.71E-11	-0.720	3.33E-03	-1.102	6.82E-17
NRXN3	1.874	1.60E-04	NS	NS	NS	NS	1.198	1.20E-02	0.909	6.89E-04
NTNG2	-0.874	7.99E-03	-1.814	3.51E-04	NS	NS	NS	NS	NS	NS
NXPE3	NS	NS	NS	NS	NS	NS	0.410	1.74E-02	0.248	2.79E-02
NXPH1	-3.019	3.98E-07	-3.666	1.84E-03	-1.338	1.06E-02	-2.317	2.46E-09	-2.892	3.11E-15
NXPH2	-2.288	5.62E-04	NS	NS	NS	NS	NS	NS	NS	NS
NXPH3	NS	NS	-2.225	1.49E-03	-1.084	7.92E-03	NS	NS	-0.675	2.66E-02
NXPH4	-2.186	5.96E-03	4.095	4.08E-14	NS	NS	-1.560	1.09E-02	NS	NS
PTPRZ1	NS	NS	-2.967	2.60E-05	-0.792	4.13E-03	-0.870	5.38E-03	-1.296	2.41E-11
RGS4	-1.982	6.80E-05	2.184	3.97E-04	1.105	7.04E-04	-1.419	2.64E-03	NS	NS
SLITRK2	-6.812	1.35E-04	NS	NS	-7.307	7.51E-25	-9.321	5.54E-06	-6.138	5.52E-14
SLITRK3	-2.958	2.68E-03	NS	NS	-1.698	6.37E-04	-3.490	1.61E-11	-2.502	6.76E-07
SLITRK4	-4.157	7.12E-05	NS	NS	-3.713	5.02E-05	-2.678	1.20E-02	-2.457	5.86E-05
SLITRK5	-2.047	3.87E-07	NS	NS	-1.184	1.54E-06	-1.734	9.31E-08	-1.152	1.05E-08
SPARCL1	-2.314	6.14E-06	NS	NS	NS	NS	-0.843	3.87E-02	NS	NS
TNR	-3.082	8.83E-06	-5.108	1.89E-07	-2.227	8.81E-13	NS	NS	-2.137	5.56E-12

Genomic analysis of SCZ-derived hGPCs from 4 different patients revealed the significant and shared down-regulation in these cells of a number of synaptic genes, including neuroligin-3, neuroexophilin-1, LINGO1 and DSCAML1, relative to their normal controls (*red*, upregulated in SCZ vs CTRL; *green*, downregulated in SCZ GPCs; color intensity proportionate to differential dysregulation). Other synapse-associated genes, such as the SLITRKs 2-5, were significantly and sharply downregulated in GPCs derived from 3 of the 4 patients (lines 8, 51 and 164).

Lines 08, 29, 51 and 164: schizophrenia-derived, different patients; pooled controls, 3 lines, each from a different patient. Individual SCZ line data shown as well as pooled SCZ data, to highlight both commonalities and distinctions between SCZ GPCs derived from different patients. Log2FC: $\log_2$ fold-change in expression. NS: not significant.